Energy & Buildings 296 (2023) 113324

Contents lists available at ScienceDirect

Energy & Buildings

journal homepage: www.elsevier.com/locate/enbuild

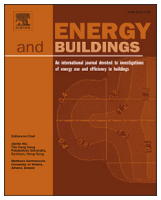

Modelling the impact of an urban development project on microclimate and outdoor thermal comfort in a mid-latitude city

Julian Anders [a,c,*], Sebastian Schubert [a,b], Tobias Sauter [a], Siiri Tunn [a], Christoph Schneider [a], Mohamed Salim [a,b,d]

[a] Humboldt-Universität zu Berlin, Unter den Linden 6, Berlin, 10099, Germany
[b] Technische Universität Berlin, Straße des 17. Juni 135, Berlin, 10623, Germany
[c] Leibniz Universität Hannover, Welfengarten 1, Hannover, 30167, Germany
[d] Aswan University, Sahary city, airport road, Aswan, 81528, Egypt

ARTICLE INFO

Keywords:
Microclimate
PALM-4U
Outdoor thermal comfort
PET
Development
Urban planning

ABSTRACT

This study assesses the impacts of sustainable urban development adapted to climate change in the city of Stuttgart, Germany. We use the state-of-the-art meteorological modelling system PALM-4U to simulate the microclimate and outdoor thermal comfort of the development site Neckarpark during a heatwave. We compare the atmospheric conditions of the current urban structure before the development project (2018) and the future state, representing the new district after completion (2025). Our results indicate that the restructuring barely affects surrounding neighbourhoods, but leads to mean near-surface air temperature increases in the centre of development between +0.25 K and +2 K. Differences in Physiologically Equivalent Temperature (PET) show a heterogeneous pattern at daytime, with a large amplitude and temporal variability in the diurnal cycle (−9 K to +12 K). At night, the planned buildings increase the mean PET by +1 K to +6 K. The new buildings reduce the effect of adaptation measures designed to increase the cooling effects, i.e. urban trees and vegetation, amplifying the thermal stress during heatwaves. Our study confirms the complex composite impacts of urban restructuring due to the thermal and dynamic flow processes. The paper may serve as a guide for the use of meteorological models to assess microclimatic impacts of planned development projects, contributing to urban planning and adaptation strategies.

1. Introduction

Urban environments are spaces of paramount importance given their high concentration of population and infrastructure, their key function in political, economic and social processes, and their immanent vulnerability [9]. Nowadays, more than half of the world's population resides in cities, and it is estimated that urban population will exceed 68 % by 2050 [86]. Growing world population, ongoing urbanisation, and climate change exert pressure on cities and thus reinforce the need for urban adaption strategies and more sustainable planning concepts [15]. Besides the increasing frequency and intensity of extreme events worldwide, global warming is also projected to have a negative impact on human health, with urban heat islands potentially amplifying the effects of heatwaves in urban areas [42,40]. Thus, urban development projects should mitigate the urban heat island effects as much as possible [70,28,55,35].

Generally, urban climates are characterised by high temporal and spatial variability of meteorological variables due to the heterogeneity of the underlying structures, e.g. land cover, surface roughness, 3-d structures, height differences, and surface albedo [14,63,61,50,75]. Urban environments modify the local climate, which is shaped by synoptic-scale conditions and determine the background climate of a specific location [64]. Oke [62] found that the interplay of artificial urban surfaces and vegetation creates distinct micro- to local-scale climates that contribute to a mosaic of microclimates at the spatial scale of entire cities. Therefore, a prerequisite of effective urban planning is a profound understanding of the physical surface-atmosphere interaction at macro-scale (2000 km to 10 000 km), meso-scale (2 km to 2000 km), and micro-scale (< 2 km) [65].

* Corresponding author.
E-mail address: anders@meteo.uni-hannover.de (J. Anders).

https://doi.org/10.1016/j.enbuild.2023.113324
Received 14 December 2022; Received in revised form 17 March 2023; Accepted 26 June 2023
Available online 16 July 2023

The Implementation of urban development projects is often associated with changes of local surface properties, which in turn affect the energy balance and wind circulation [90,32]. In terms of urban redevelopment and thermal comfort, studies often either address the meso-scale effects of urban expansion or micro-scale effects of specific urban configurations (e.g. [1,41,23,38,84,37]), and single objects (e.g. [85,8]). Ketterer and Matzarakis [47] examined heat stress reduction by re-planning measures in a similar study design. Koch et al. [51] studied the effects on air temperature in a brownfield redevelopment project. Urban planning often considers certain effects of specific building arrangements and urban greening, however, their actual micro-scale and composite impacts are still not fully understood.

Urban Climate Models (UCMs) represent a tool to support emerging building technologies that hold great potential for mitigating climate change and conserving energy in urban areas. Given the long-term and often irreversible nature of urban planning decisions, UCMs have become a powerful tool for urban planners [19]. Over the past few decades, the scientific community has developed several numerical models for urban applications, including ENVI-met [11], MUKLIMO_3 [27], MITRAS [77], ASMUS [34], and UrbClim [74].

PALM-4U (**PA**rallelised **L**arge-eddy simulation **M**odel for **U**rban applications) is a modern UCM system, developed specifically for use in urban climate studies. It has been designed to cater to various urban applications, ranging from meso-scale to micro-scale [71,58]. Large-eddy simulation (LES) models like PALM-4U offer the potential of more accurate and reliable results compared to Reynolds-Averaged-Navier-Stokes models, as they can resolve temporal 3-d fluctuations, and the flow around obstacles in an urban environment [56,91,10]. Moreover, PALM-4U is fully parallelised, resulting in high scalability [59]. The model has been increasingly used for various urban applications, including modelling of turbulence and wind fields [67,66], aerosol concentrations [46], and biometeorological thermal exposure [31,30].

In this study, our objective is to examine the impact of a planned development project on the microclimate and outdoor thermal comfort in a mid-latitude city. A $0.22\,km^2$ area of predominantly bare soil is to be redeveloped into an area of new buildings, parks, trees, and streets. To assess the effects of this development, we compare high-resolution simulations of the current state with those – based on development plans – of the future state [2]. To achieve this, we use the state-of-the-art open-source model PALM-4U and force it with realistic meteorological conditions in a nested holistic approach [43]. We use the June 2019 heatwave as a surrogate for future events and apply large-scale forcing as a boundary condition for the model. By doing so, we aim to quantify and trace the microclimatic impacts resulting from structural urban changes. Our work here also serves as a guide regarding using this method to identify the impact of new urban development projects on the microclimate.

2. Material and methods

2.1. Study area

The study area (centred at 48.796 °N, 9.225 °E) is located in the city of Stuttgart in the southwest of Germany (Fig. 1). According to Köppen [52], the prevailing climate is characterised by a humid warm temperate climate (*Cfb*).

2019 is the second warmest year in Germany since 1881, with an average air temperature of 10.3 °C. Overall, the year was characterised by rather dry conditions (93% of the long-term average), more sunshine than usual, and extreme heat waves during summer [22]. The heat wave in late June occurred as a result of a high-pressure ridge across Western Europe and a low-pressure system that developed offshore the Iberian peninsula, inducing intense advection of hot air from North Africa to Europe [88].

The regional climate of Stuttgart is shaped by its topographical position in the Neckar basin, shielded by the Black Forest in the west, the Swabian Alb in the south, the Schurwald forest in the east, and the local Strom- and Heuchelberg low mountain areas in the northwest [6]. Stuttgart is one of the warmest regions in Germany with comparably low precipitation due to surrounding low mountain ranges and their shielding effects. The citizens are exposed to strong urban heat island (UHI) effects and strong air pollution, which is connected to weather conditions with low wind speeds and air temperature inversions [48].

The urban development project investigated aims at restructuring the Neckarpark site, which is located in the northeast of Stuttgart. The study area is currently restructured and is intended to undergo a transformation from an abandoned former railway area to a sustainable district.[1] The area under construction covers $0.22\,km^2$ and is scheduled for completion by 2025 [3,2].

2.1.1. Current study area (2018)

When referring to the 'current study area' or the 'current scenario', we refer to the state in 2018 (Fig. 2a). The north-facing study area is enclosed by railroad tracks from north to east and a river in the southwest. Terrain height in the model domain ranges from 268 m above sea level in the southwest to 282 m above sea level in the northeast.

According to the classification system by Stewart and Oke [82], the Neckarpark development site can be classified as compact midrise (LCZ 2) or open midrise local climate zone (LCZ 5) with scattered trees (LCZ B), i.e. LCZ 2_B or LCZ 5_B. Most buildings are concentrated in the north of the current study area, mainly comprising residential and office buildings that were built before 1950. Most buildings range between approx. 7 m and 13 m, with the tallest building exceeding 23 m in height. Current vegetation consists primarily of short grass in courtyards and parks and single trees located along main streets and the river. The centre of the current study area is characterised by bare soil.

2.1.2. Future study area (2025)

When referring to the 'future study area' or the 'future scenario', we refer to the state in 2025 after completion of the development project (Fig. 2b). The centre of the study area undergoes the most pronounced transformation. Major changes arise from several newly constructed buildings replacing the former bare soil. These are almost exclusively new residential buildings, which have higher insulation standard than the surrounding older buildings. Most building complexes have inner courtyard structures interspersed with short grass and single trees. The existing older buildings in the centre are to be refurbished and their insulation standard improved. Around the new buildings there are new areas with short grass. However, some buildings in the northeast and in the southeast disappear. Additional minor structural changes occur due to the rearrangement of some older buildings, affecting the network of roads and walkways. In total, the number of single trees increases by 591, which are mainly located along main roads, in emerging parks and recreation areas, and inner courtyards. In summary, both sealed surfaces and vegetated ares with trees increase at the expense of bare soil in the future scenario.

2.2. PALM-4U

PALM-4U[2] is a modern and highly efficient UCM allowing for simulations of the urban atmosphere with building-resolving spatial resolution over a neighbourhood and a city scale [57,76]. PALM-4U solves the 3-d, non-hydrostatic, filtered, incompressible Navier–Stokes equations of wind and scalar variables. The model applies the Boussinesq approximation to the filtered Navier–Stokes equations to neglect the density variations for the buoyancy term.

This model is equipped with all the modules required for simulating urban areas, such as the plant canopy module [44], the urban

[1] https://www.stuttgart-meine-stadt.de/stadtentwicklung/neckarpark/.
[2] https://palm.muk.uni-hannover.de/trac/wiki/doc/tec.

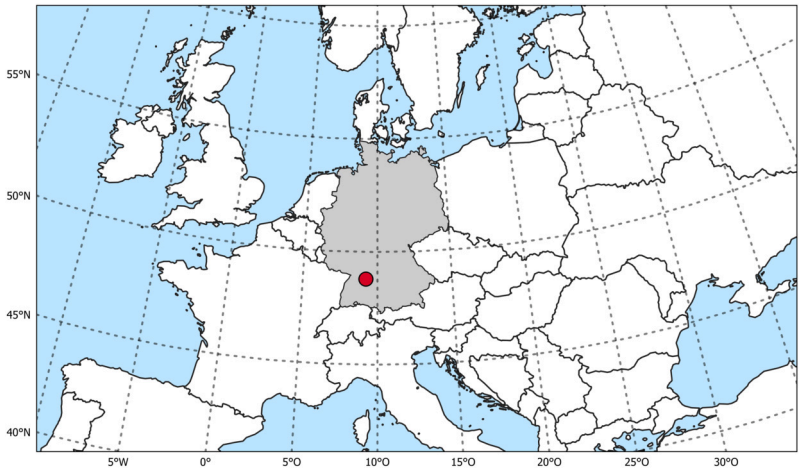

Fig. 1. Topographic location of the Neckarpark urban development site in Stuttgart, Germany.

(a) Current Study Area (2018)

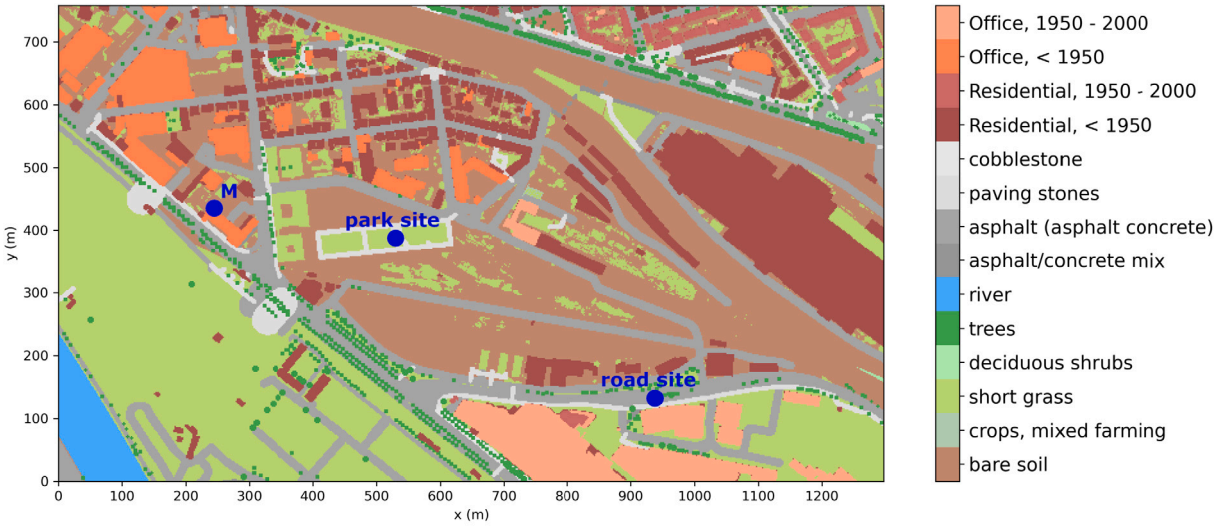

(b) Future Study Area (2025)

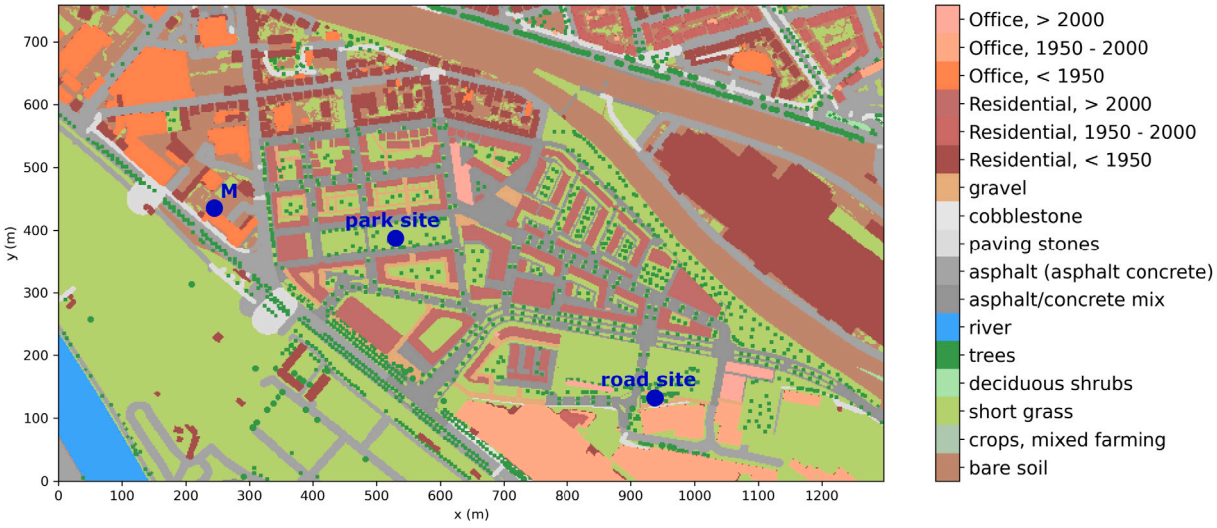

Fig. 2. Spatial delimitation of the Neckarpark development site showing (a) the current study area (2018) and (b) the future study area (2025). The location of the local measuring station is shown as *M* in blue and the specific sites *park site* and the *road site* are displayed in blue at the map. (For interpretation of the colours in the figure(s), the reader is referred to the web version of this article.)

surface module [73], the land surface module [29], the radiation module [53,78], the indoor climate module [69], the chemistry module [49], and the biometeorological module [26]. The model has been successfully evaluated against field measurements [72,7], wind tunnel simulations [33], and previous LES studies [68]. It shows also excellent scalability on massively parallel computer architectures [59]. As computing resources, we use cluster nodes with Intel Xeon E5-2630v4 chips running at 2.2 GHz that are connected via Intel OmniPath. For each scenario we use 500 cores resulting in a running time of approx. 40 hours.

2.2.1. Model setup and boundary conditions

We define a horizontal grid spacing of 2 m to capture microclimatic effects at the micro-γ-scale [25]. The model domain covers an area of 1300×760 m, i.e. 650×380 grid cells. We use a vertical grid spacing of 2 m below 90 m and apply a stretch factor of 1.02 above 90 m. Atmospheric processes are resolved up a height level of approx. 3000 m, with a subdivision into 350 height levels.

The modelling period is 24 hours, using meteorological input from 30 June 2019, beginning at midnight (00:00 UTC). The day is during a heatwave and characterised by clear-sky conditions. Prior to the actual 3-d atmosphere simulation, a spin-up phase of 24 hours is preceded for adjusting the inert soil- and wall-layer temperature to the prevailing atmospheric conditions. Spin-up is initialised by using meteorological conditions of the previous day. During spin-up phase, the soil and wall modules run without an interactive atmosphere.

PALM-4U uses 1.5-order turbulence closure to explicitly solve the turbulent motions in the atmospheric boundary layer [59]. A multigrid scheme (w-cycle) and the discrete Fourier transformation (FFTW) routine is used for solving the Poisson equation for the perturbation pressure, with calculations at every Runge-Kutta step. The advection terms are discretised using an upwind-biased 5th-order differencing scheme in combination with a 3rd-order Runge–Kutta time-stepping scheme [89].

Energy balance solvers for interactive building and paved surfaces are switched on. The simulation is carried out with non-cyclic boundary conditions and Dirichlet conditions for potential temperature and humidity. For both the horizontal velocity components and the subgrid-scale turbulence kinetic energy we use Dirichlet no-slip boundary conditions. The external Rapid Radiation Transfer Model for Global Models (RRTMG) is used to calculate the radiative heating rates for each model column [17].

Data from the non-hydrostatic regional model COSMO (**CO**nsortium for **S**mall-Scale **MO**delling) developed at the German Meteorological Service provide the initial and boundary conditions[3] [81,20].

The COSMO model has been designed for operational numerical weather prediction and various scientific applications on the meso-β-scale and meso-γ-scale. We use hourly data from COSMO-D2, a higher-resolution short-term forecasting model of the COSMO model system. It covers Germany, Switzerland, Austria, and parts of neighbouring countries and has a horizontal grid spacing of 2.2 km [4,79]. We interpolate the COSMO data both spatially and temporally to match the model setup by applying the meso-scale interface for **INI**tialising and **FOR**cing PALM (INIFOR) [43].

We use the same model setup and meteorological boundary conditions for both the current and the future scenario to attribute the microclimatic changes to the modification of urban structures. Thus, the impacts of climate change are not included in the meteorological forcing.

[3] https://www.cosmo-model.org/content/model/documentation/core/default.htm.

2.2.2. Surface description

As described in detail by Heldens et al. [36], PALM-4U requires surface parameters of buildings, vegetation, soil type, terrain height, and further urban infrastructures.

We obtain all geospatial data for the current study area from the German aerospace centre, Deutsches Zentrum für Luft- und Raumfahrt (DLR). We verify the data quality, modify erroneous classifications, and add missing information by using latest satellite imagery. The DLR acquired building data from local municipalities, 3-d model City Geography Markup Language (CityGML), and the 3-d triangulated irregular network [80]. This resulted in detailed information about building height, roof slope, and building function. DLR sources for infrastructure and vegetation were OpenStreetMap[4] and CORINE land cover data [18]. Both OpenStreetMap and CORINE data can contain errors of omission and commission, leading to potential misclassifications, especially when used as a source of high-resolution urban information. However, several studies validated their quality against ortho-corrected high spatial resolution satellite images and land use/land cover datasets (e.g. [13,12,24]). The implementation of the future study area requires fundamental editing. We create the future scenario based on the construction plans of the Office for Urban Planning and Housing of Stuttgart. These construction plans contain information about residential areas, traffic areas, green spaces, industrial estate, infrastructural area, and tree locations. However, the construction plans have no information about exact building shapes and heights, courtyards, single tree characteristics, smaller pathways, types of emerging roads, park trials, and pavements. Thus, we adapt the construction plans by inserting building shapes, paths, single trees, and green patches, as illustrated on the commercial photo of the official project website[5] (Fig. B.8). A detailed visualisation of construction plans and the manually induced changes can be found in the supplementary materials (Fig. B.9).

We make assumptions regarding the characteristics of the new urban elements. Newly implemented buildings are distinguished by residential buildings with heights of 12 m or 16 m and office buildings with heights of 6 m or 8 m height. The assigned building types correspond to parameterisations of energetic properties, as described by Heldens et al. [36]. The classes are derived by building use and age and differ mainly in the fraction of building components and their thermodynamic characteristics. Not only new buildings are added, but also some old buildings are removed, which is due to a trade-off between latest data (current scenario) and an idealised vision of the future scenario. In terms of vegetation, we combine non-resolved (i.e. flat) vegetation surfaces with uniform properties and single trees that are resolved in 3-d by the numerical grid. The former is used for larger vegetation patches in courtyards and parks. All single trees added are type Acer (height: 12 m, crown diameter: 7 m, LAI summer: 3.0) as it is the most frequently occurring tree type in the centre of Stuttgart.[6]

2.3. Evaluation of PALM-4U

For evaluation, we compare the PALM-4U output of the current situation (*PALM*) with meteorological observations (*OBS*) and the meso-scale forcing data (*COSMO*). We evaluate the simulations with averaged 30-min meteorological observations within the model domain (Fig. 2, Point **M**).[7] The measuring station is located on a 15 m high roof and is surrounded by buildings, sealed area, and nearly no vegetation. In order to compare the diurnal cycle between the weather station and the model, we extract the air temperature at the roof top level where the station is located.

[4] https://planet.openstreetmap.org/.
[5] https://www.stuttgart-meine-stadt.de/stadtentwicklung/neckarpark/.
[6] https://www.stuttgart.de/leben/bauen/geoportal/stadtplan-stuttgart.php.
[7] https://www.stadtklima-stuttgart.de/index.php?klima_messdaten_station_fw.

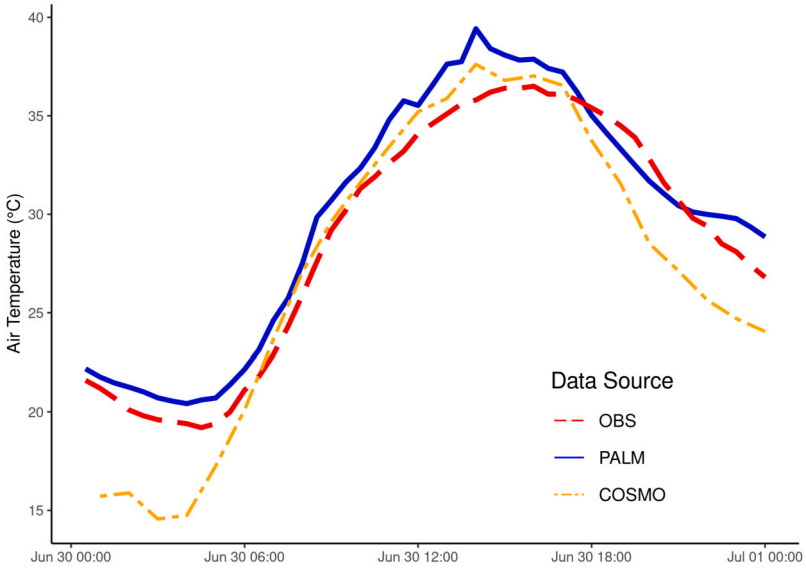

Fig. 3. Evaluation of the PALM-4U model output for the current situation (*PALM*) by comparing the near-surface air temperature to local measuring data (*OBS*) and the meso-scale COSMO forcing data (*COSMO*). Diurnal air temperature cycles correspond to UTC timecode.

2.4. Microclimatic changes

We calculate the scenario effects by subtracting the PALM-4U output of the current scenario from the future scenario. We mask out all buildings, even if they only exist in one of the two scenarios. Separation into daytime and nighttime is based on sunrise (03:30 UTC) and sunset (19:30 UTC). In order to assess whether these scenario effects differ significantly from zero, we perform a two-sample *t*-test for auto-correlated data as described by Zwiers and Storch [92].

Besides the near-surface air temperature, we investigate the outdoor thermal comfort using the physiologically equivalent temperature (PET) [39]. The PET is a biometeorological index that translates an indoor reference climate into outdoor conditions, incorporating the human-body energy balance and meteorological conditions, namely mean radiant temperature, air velocity, air humidity, and air temperature [39,60,85].

Finally, we investigate how scenario changes affect the microclimate of two specific sites, the *park site* and *road site* marked in Fig. 2. The *park site* is located in the park in the centre and is covered by short grass in both scenarios, but with different environmental conditions in the surrounding region. While the park in the current scenario is enclosed by bare area, it is surrounded by residential buildings, sealed pavements/streets, and interspersed with nearby trees in the future situation. The *road site* is converted from a main road (current) to a green space with short grass and several adjacent trees (future).

3. Results

3.1. Evaluation of PALM-4U

By dynamically downscaling the meso-scale COSMO forcing data to the micro-scale using PALM-4U, we considerably improve the diurnal cycle of the near-surface air temperature (Fig. 3). *PALM* consistently shows a higher near-surface air temperature than *COSMO* at all times of the day. While the temperature curves align quite close during the day with maximum differences of −2 K, *COSMO* reveals a much colder air temperature during the nighttime with maximum differences of −5.8 K. Furthermore, the air temperature of *PALM* drops at a much lower rate after 18:00 UTC. Overall, *COSMO* shows a high daily amplitude (23.1 K) which is lower for *PALM* (19.2 K) and also for *OBS* (17.3 K).

PALM and *OBS* show a significant correlation of 0.987 (p-value< 0.01). However, *PALM* overestimates the air temperatures, in particular during noon. On average, *PALM* has a bias of +1.1 K, with a maximum overestimation of +3.8 K at 14:00 UTC. In addition to the temperature bias, the incoming shortwave radiation also differs (Fig. B.12), as *PALM* has a higher mean radiation (*PALM*: 360 W m^{-2}, *OBS*: 341 W m^{-2}) and a higher maximum (*PALM*: 927 W m^{-2}, *OBS*: 888 W m^{-2}).

3.2. Microclimatic changes

3.2.1. Near-surface air temperature

The near-surface air temperature ranges from 17 °C before sunrise to a maximum peak of 42 °C during afternoon in both scenarios. Mean air temperature differences of the future and the current scenario are depicted in Fig. 4, separated by day (Fig. 4a) and night (Fig. 4b). For more details on the diurnal cycles of the absolute temperature, see the appendix (Fig. B.13, Fig. B.14).

Both the daytime and nighttime situations show a similar heterogeneous spatial temperature pattern, with a higher temperature amplitude during the daytime (−2.3 K to +3.5 K) compared to the nighttime (−2.3 K to +2.1 K). Temperature increases primarily in the centre of the study area. Temperature changes are on average more than +0.5 K during daytime and often exceed +1.0 K, or even +1.5 K at locations close to the new buildings. The nighttime overall shows the same pattern with less pronounced differences. However, the area influenced by the development project seems to be greater during the night with increases of +0.25 K to +0.5 K.

Along a narrow band adjacent to the east and south of the new residential area, temperatures are cooler than in the reference run. While the changes are moderate at daytime (−0.5 K to −1.0 K), they become more prominent at nighttime (−0.5 K to −2.0 K). Some locations even exceed −2.0 K. Outside the model domain centre, most locations remain unchanged on average (less than ±0.25 K), especially during daytime. Noticeable, there is an area in the southeast, bare soil (current) converted to a park (future), that shows positive changes during the day and negative ones at night.

Fig. 4c shows the two-sample *t*-test for auto-correlated data. Significant changes (p-value < 0.05) are found in the centre, coinciding with the development area. Further significant changes can be found mainly in the northwest, north, and northeast of the centre.

3.2.2. Outdoor thermal comfort

The PET ranges from 10 °C to 62 °C in both scenarios. Fig. 5 shows the mean PET differences between future and current scenario. In the

(a) Daytime mean air temperature differences

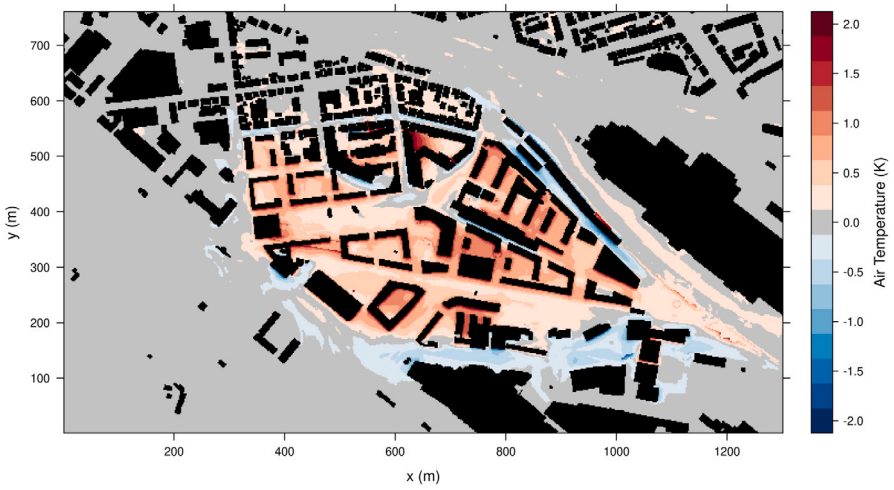

(b) Nighttime mean air temperature differences

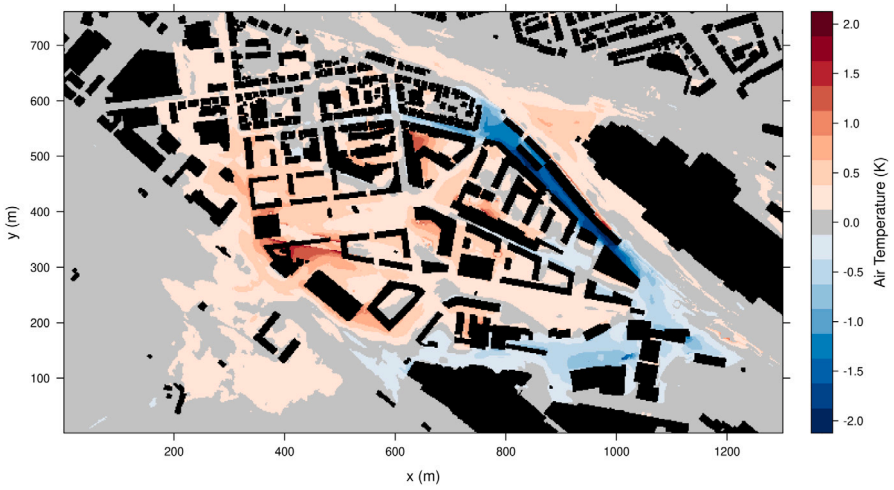

(c) Two-sample t-test for auto-correlated data

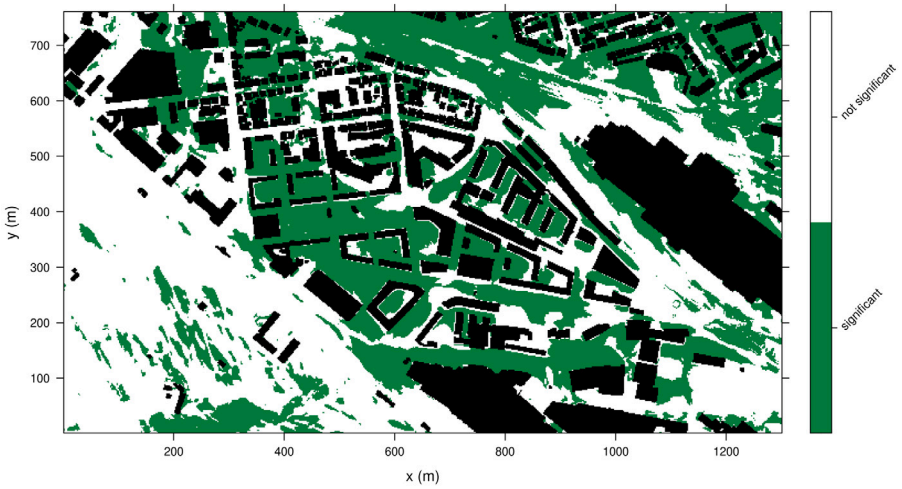

Fig. 4. Mean near-surface air temperature differences between the two scenarios at (a) daytime (03:30 – 19:30 UTC) and (b) nighttime (19:40 – 03:20 UTC). Statistical significance (c) is based on a two-sample t-test for auto-correlated data (green colour: statistically significant, p-value < 0.05). Black objects are buildings in at least one of the two scenarios.

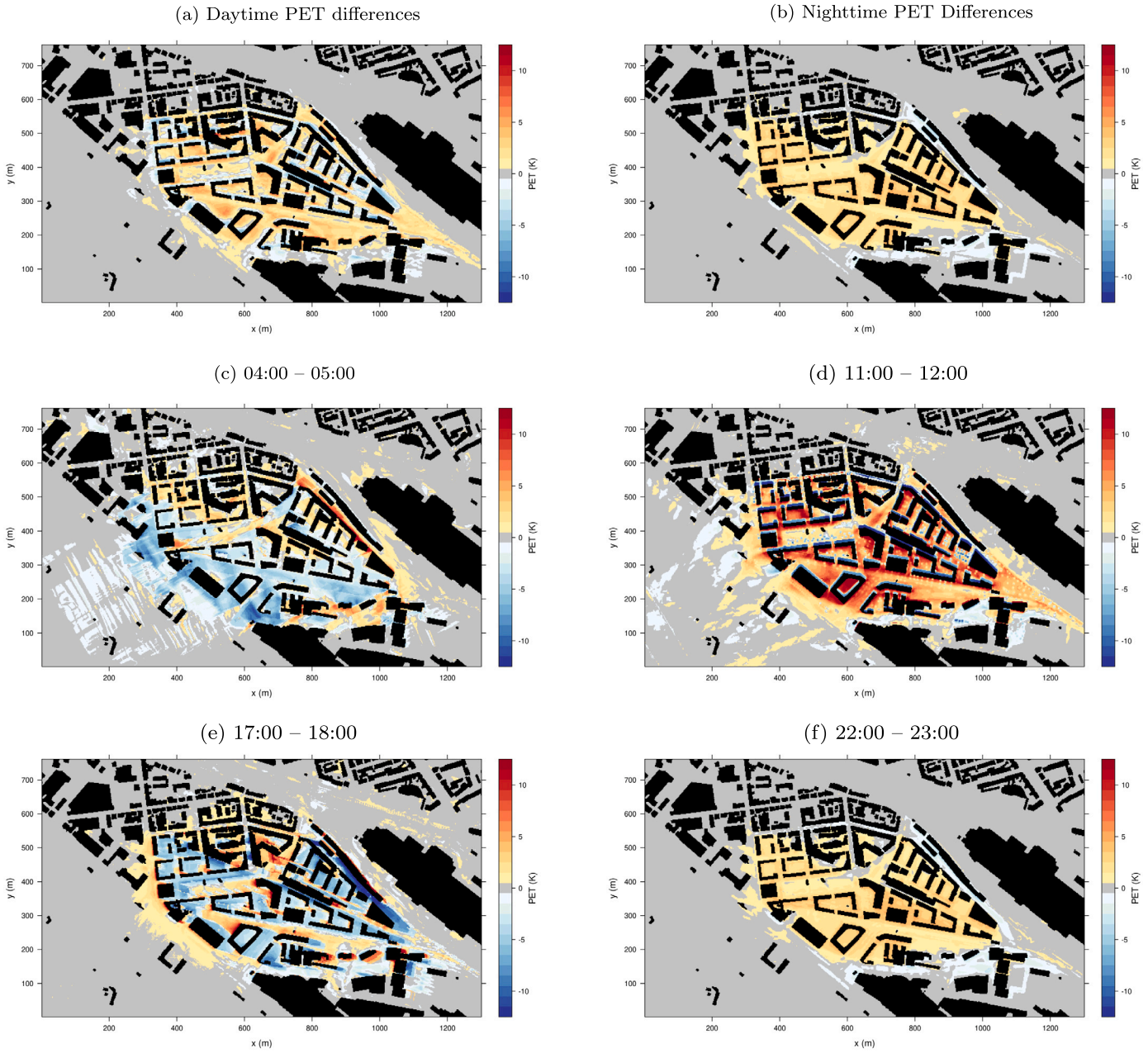

Fig. 5. Mean physiologically equivalent temperature differences between the two scenarios, showing (a) daytime difference (03:30 – 19:30 UTC), (b) nighttime difference (19:40 – 03:20 UTC), and hourly averaged differences between (c) 04:00 – 05:00, (d) 11:00 – 12:00, (e) 17:00 – 18:00, and (f) 22:00 – 23:00 UTC. Black objects are buildings in at least one of the two scenarios.

future scenario, the PET increases during daytime and even more in the night situation. Similarly to the air temperature, the amplitude is higher during the day (−8.9 K to +12.2 K) compared to the night situation (−5.1 K to +6.0 K). The amplitude of instantaneous (non-averaged) PET differences even exceeds ±20 K at single locations during the day. For more details on the diurnal PET cycles, see the appendix (Fig. B.15, Fig. B.16).

While an enhanced but inconsistent PET pattern occurs in the core area of the model during the day, the PET increases at night (+1.0 K to +6.0 K). An exception are the band-shaped negative PET changes, which are consistent with the air temperature pattern. During the day, courtyards enclosed by tall buildings, narrow street canyons, and areas north of buildings show negative PET values. Wide streets and south-facing open spaces, on the other hand, show positive PET values. Newly planted trees reduce PET extremes, e.g. along main roads or in the new green spaces.

Shortly after sunrise (Fig. 5c), negative PET changes up to −10 K primarily occur in the southern part of the centre. During late noon (Fig. 5d), the centre of the model domain is characterised by remarkably high PET values, with only negative changes in the north of buildings and scattered spots corresponding to single tree locations within parks, along streets, and in courtyards. By far, highest positive changes are achieved during the period from 11:00 – 12:00. The situation shortly before sunset (Fig. 5e) is analogous to the one before sunrise, but showing a different spatial shift of negative changes. The PET situation at 22:00 – 23:00 (Fig. 5f) corresponds to mean PET changes of the entire night.

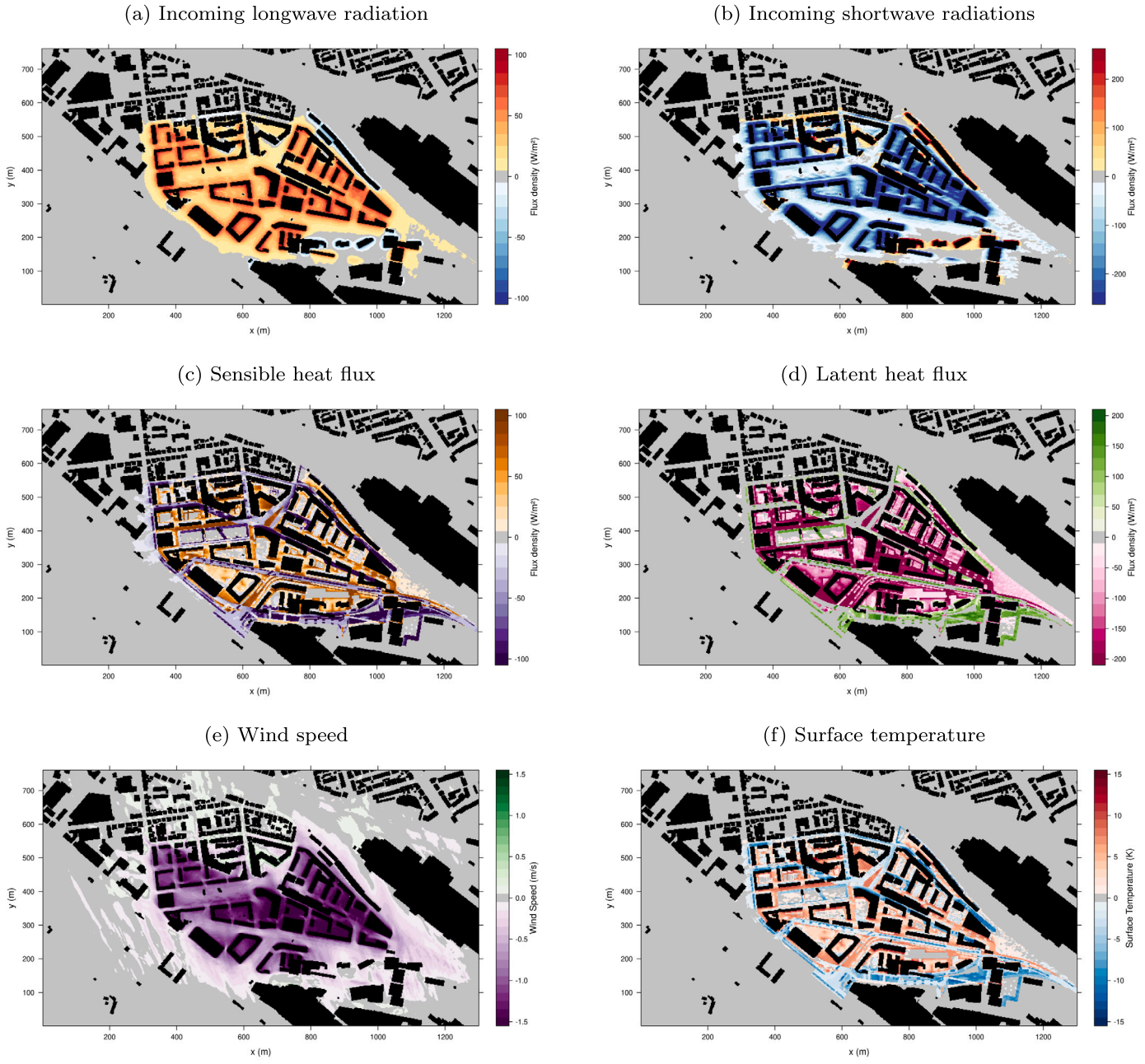

Fig. 6. Comparisons between the current state and the future scenario of the development area showing the mean differences in (a) incoming longwave radiation, (b) incoming shortwave radiation, (c) sensible heat flux, (d) latent heat flux, (e) wind velocity, and (f) surface temperature. Black objects are buildings in at least one of the two scenarios.

3.2.3. Incoming radiation, turbulent fluxes, wind velocity, and surface temperature

Differences of incoming radiation, sensible heat, latent heat, wind velocity, and surface temperature between the two scenarios are shown in Fig. 6. All variables are averaged over the modelling period.

Longwave radiation increases in the centre ($+10\,\mathrm{W\,m^{-2}}$ to $+108\,\mathrm{W\,m^{-2}}$). Small areas of negative change occur in the north-east and south-east of the centre (Fig. 6a). Incoming shortwave radiation reveals exactly the opposite pattern (Fig. 6b), as surfaces in the centre receive up to $-531\,\mathrm{W\,m^{-2}}$ less shortwave radiation in the future scenario.

In the centre of the model domain, there is a predominant shift towards more sensible (Fig. 6c) and less latent heat flux (Fig. 6d). Sensible heat flux increases due to new buildings, sealed surfaces, and streets, and decreases at emerging green spaces in the northeast, the south, and the southeast. Regardless of the overall trend, sensible heat flux changes range between $-157\,\mathrm{W\,m^{-2}}$ and $+162\,\mathrm{W\,m^{-2}}$ and latent heat flux changes between $-214\,\mathrm{W\,m^{-2}}$ and $+196\,\mathrm{W\,m^{-2}}$.

Horizontal wind velocity at 10 m decreases in the entire model domain (Fig. 6e). The centre reveals values between $-0.5\,\mathrm{m\,s^{-1}}$ and $-1.5\,\mathrm{m\,s^{-1}}$, especially around new buildings and courtyards even exceeding $-2.0\,\mathrm{m\,s^{-1}}$. Surface temperature changes show a heterogeneous pattern, with maximum differences of $\pm 24\,\mathrm{K}$ (Fig. 6f).

3.2.4. Specific sites

The diurnal cycles at specific sites are shown in Fig. 7. Here, the sign convention of the energy balance corresponds to the micrometeorological convention, i.e. net shortwave and longwave radiation are positive if they are an energy gain, latent and sensible heat flux are

(a) park site: short grass (current) to park surrounded by buildings (future)

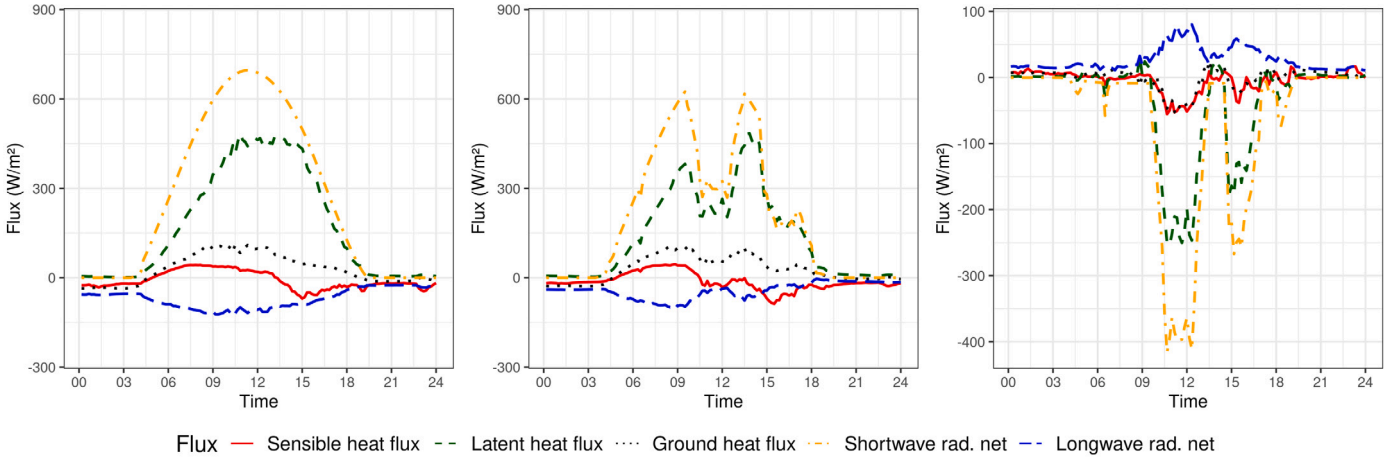

(b) road site: road (current) to short grass and nearby trees (future)

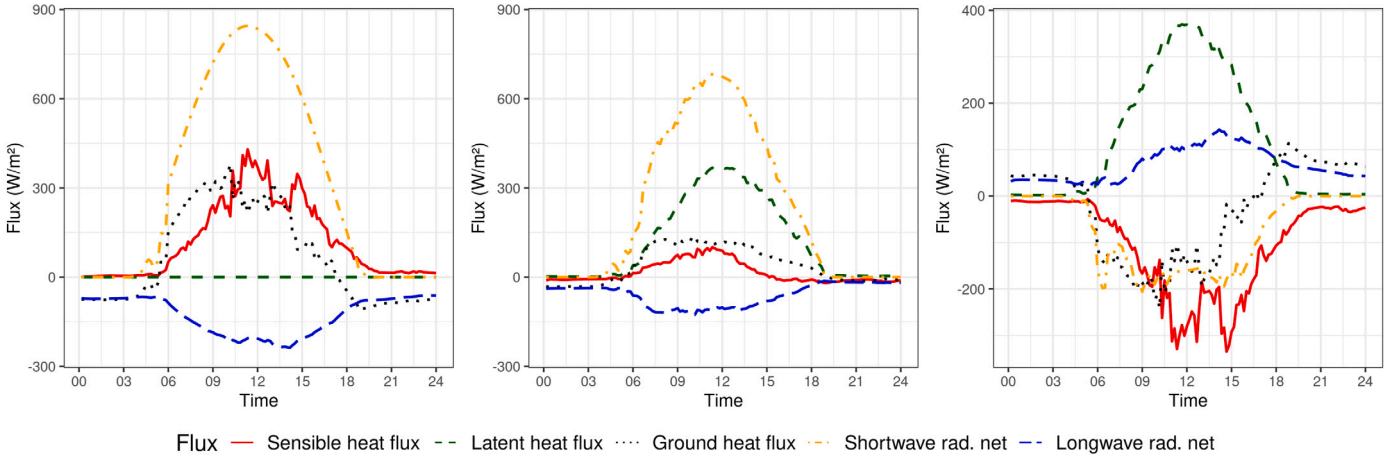

(c) Difference (future – current) in diurnal cycles for both sites

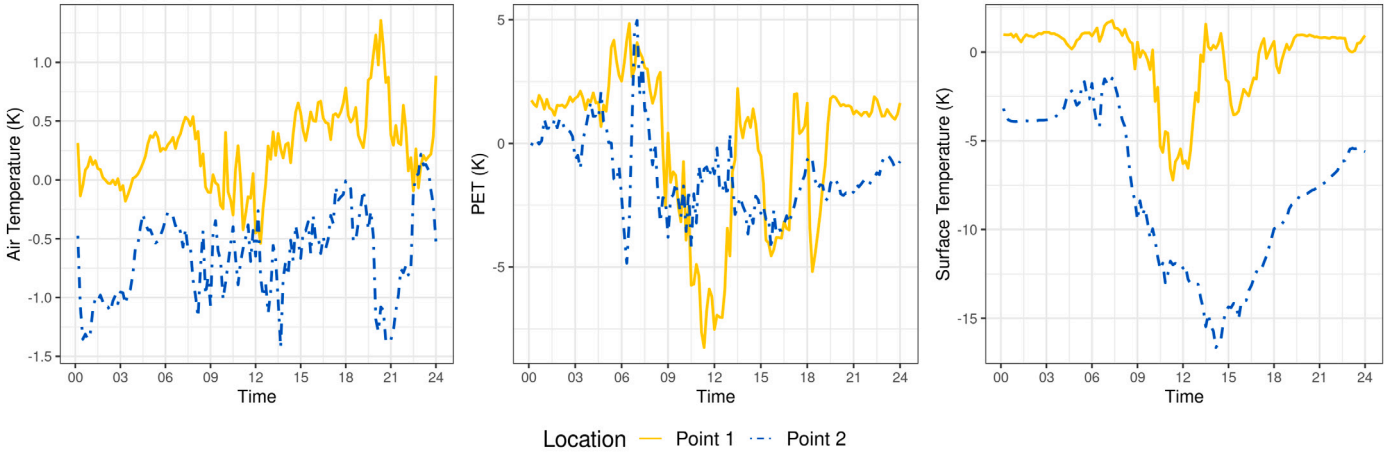

Fig. 7. Investigation of two specific sites; (a) *park site* and (b) *road site*. As marked in Fig. 2, *park site* is covered by short grass in both cases, but surrounded by bare areas (current) and buildings and trees (future), while *road site* experienced a conversion from an asphalted street to a short grass spot with nearby trees. Diurnal energy balance cycles and scenario differences are depicted for *park site* and *road site*, following micro-meteorological sign convention. Scenario differences in air temperature, PET, and surface temperature are visualised in (c).

positive if they are directed from the surface to the atmosphere, and ground heat flux is positive if heat storage at the surface and the underlying soil layers occurs.

The current scenario for the *park site* (Fig. 7a) shows a pronounced daily cycle with a high positive latent heat flux during daytime, whereas the daily cycle of the sensible heat flux is small. In the future scenario, the latent heat flux and incoming shortwave radiation decrease. When comparing both scenarios, the mean latent heat flux decreases by $-38\,W\,m^{-2}$, reaching maximum differences of $-254\,W\,m^{-2}$ around noon and afternoon. Mean net shortwave radiation also decreases by $-70\,W\,m^{-2}$, with differences exceeding $-400\,W\,m^{-2}$ between 10:30 and 12:30 and considerable high differences of more than $-250\,W\,m^{-2}$ between 14:30 and 16:00. The net longwave radiation is positive throughout the day (mean: $+27\,W\,m^{-2}$) with maximum peaks during the same time periods just described.

The *road site* shows in the current scenario (Fig. 7b) a high sensible heat flux, a strong ground heat flux, and no latent heat flux. The future situation reveals a latent heat flux in the magnitude of the former sensible heat flux. Sensible heat is reduced by more than one third, both ground heat flux and net shortwave radiation decrease, but net longwave radiation increases. Considering scenario changes, sensible heat flux on average decreases by $-105\,W\,m^{-2}$, exhibiting maximum declines of $-334\,W\,m^{-2}$, the previously non-existent latent heat on average is $+124\,W\,m^{-2}$ with a maximum of $+369\,W\,m^{-2}$ at noon. Net longwave radiation increases throughout the day (mean: $+59\,W\,m^{-2}$) and net shortwave radiation decreases (mean: $-79\,W\,m^{-2}$). Ground heat flux differences are positive during nighttime and negative during daytime.

Differences in the diurnal cycles between future and current scenario are illustrated in Fig. 7c. Air temperature at the *park site* increases in the future situation, with highest increases occurring during afternoon and after sunset (mean +0.3 K, maximum: +1.3 K). Negative air temperature changes occur at noon (minimum: −0.5 K). In contrast, the *road site* experiences colder conditions (mean: −0.6 K) in the future scenario and air temperature shows a maximum difference of −1.5 K during the night before sunrise, after noon, and during sunset. PET reveals a higher variation and amplitude of changes. The *park site* shows positive PET changes of around +2 K during the night and in the morning (maximum: +4.8 K) but also has three periods (09:00 – 13:00, 15:00 – 17:00, and 18:00 – 19:30) with negative lowpoints of −8.2 K, −4.5 K, and −5.2 K, respectively. Nearly consistent negative changes (mean: −1.1 K) occur at the *road site*, corresponding to lower future PET values. The change in surface temperature at the *park site* corresponds to the trajectory of the PET curve. The *road site* consistently reveals negative surface temperature values with maximum differences of −16.4 K during afternoon.

4. Discussion

4.1. Evaluation of PALM-4U output

Air temperature differences between *COSMO* and *PALM* can be attributed to the simplistic urban parameterisation and the coarser grid spacing of the meso-scale *COSMO* forcing data. *COSMO* uses simple land cover parameterisations and poorly represents urban environments [21]. The model sensitivity to the large-scale weather pattern in the forcing data is recognisable in the diurnal cycles, especially during daytime. It is noticeable that already the *COSMO* shows a higher air temperature during the day than *OBS*. However, dynamical downscaling of the coarser *COSMO* data with PALM-4U by inserting geospatial urban information considerably improves the diurnal cycle, as can be seen in the small differences between *PALM* and *OBS*. *PALM* has a positive temperature bias throughout the entire model period. Nonetheless, the diurnal cycle is captured quite well, as the deviation from *OBS* is +1.1 K on average. Similar maximum discrepancies in the diurnal cycle (± 3 K) were also observed in the validation study of Resler et al. [72].

The higher incoming shortwave radiation of *PALM* in comparison to *OBS* has a strong impact on the energy balance and propagates to the simulations. Air temperature before sunset is influenced by the spin-up phase, which is mainly driven by radiation. Consequently, higher incoming radiation translates into a warmer spin-up phase and thus increases heat storage and higher soil/building temperature. This in turn heats the air layer above at the onset of the modelled day. Shortwave radiation differences are also most prominent during noon, which fits to the observed maximum temperature differences. Potential error sources could be related to parameterisations of the components determining the energy balances of certain locations (e.g. albedo, longwave radiation), which then could be reflected in the turbulent fluxes. Conclusively, differences in incoming shortwave radiation appear to be mainly responsible for the temperature bias. However, since we are interested in the differences between the scenarios, this bias is not problematic for this study.

In addition, several studies validated important meteorological variables that determine thermal comfort, i.e. wind flow (e.g. [33,54]), radiation [53,78], and biometeorology indices [26].

4.2. Microclimatic changes

4.2.1. Near-surface air temperature

Differences in near-surface air temperature occur primarily in the centre at the locations directly affected by the scenario changes, while the surrounding area remains largely unchanged. This result indicates that urban changes have limited impact on adjacent urban spaces, and new constructions on bare ground or wasteland hardly influence the surrounding urban areas.

The air temperature differences can be attributed to the reconstruction measures of the buildings. Thermally massive building structures absorb, store, and emit more energy from solar radiation per unit area than bare ground. The surface energy budget quickly responds to these changes and the radiative (Fig. 6a, 6b) and turbulent sensible heat flux (Fig. 6c) heat the near-surface layer and determine the temperature distribution in the street canyons. Generally, the sensible heat flux increases at the expense of the latent heat flux (Fig. 6d), as the proportion of green spaces in the vicinity of the new buildings decreases. Heat traps occur mainly in courtyards or between buildings, where low sky-view-factors reduce heat exchange and long-wave radiation losses [63,83,87]. The buildings also block the air flow in the street canyons, which further reduces the exchange and ventilation [16].

The results are consistent with findings from previous studies. In a similar redevelopment study in Rome ($0.09\,km^2$, Italy), an increase in air temperature between +2.5 K and +3.5 K was observed by adding new buildings [5]. When the building structure was loosened with vegetation-covered open spaces, the temperature increase was reduced between +0.5 K and +2.0 K. In a similar brownfield redevelopment project ($0.12\,km^2$), Koch et al. [51] simulated the impact of new residential buildings at the micro-scale. They found air temperature reductions of −0.5 K and −1.0 K in the centre during daytime, air temperature reductions of −1.0 K during nighttime, and overall more widespread influence on neighbouring districts. Berardi and Wang [8] also found that new buildings reduce air temperature by up to −0.9 K during the day. In both studies, the decrease in air temperature during the day was attributed to the effects of shading and higher wind speeds around the buildings. The latter was not observed in our study, most likely due to the asymmetric building layout, the higher number of implemented buildings, and the higher building density.

The band-shaped area, south and north-east to south-east of the residential centre, with a strong decrease in air temperature is converted

from buildings, roads, and pavements (current) to a green belt with individual trees (future). The conversion of the areas leads to an increase in albedo and thus to lower surface temperatures. The lower surface temperatures decrease the sensible heat flux, but at the same time increase the latent heat flux. The finding that the air temperature changes in the new park in the southeast are positive during the day but negative at night is consistent with the study of Geletič et al. [31].

The two-sample *t*-test for auto-correlated data compares the mean difference (future – current) and spread around the statistical mean. It follows that even small differences can be statistically significant if a site is characterised by lower air temperature variability. Statistical significant regions are found at sites that have undergone structural urban changes. Here, the significance test is only based on one single modelling day, which results in a very low effective sample size after correcting for auto-correlation. Longer modelling periods and/or more scenario simulations would be necessary to increase the robustness of the significance measure.

4.2.2. Outdoor thermal comfort

The PET depends on the air temperature, the mean radiant temperature, wind velocity, and humidity, and thus responds quickly to changing meteorological conditions. Negative PET changes, i.e. colder conditions in the future scenario, are primarily attributed to shading by buildings and trees, as they strongly reduce the mean radiant temperature. The diurnal cycle of the sun and the resulting sun angles mainly determine the diurnal PET cycle. Consequently, negative PET values arise near buildings and trees (Fig. 5c, 5d, 5e). This is supported by our findings that the entire new residential area receives less incoming shortwave radiation in the future scenario (Fig. 6b). Shading also explains lower mean PET values during the day at the north-side of buildings.

These results are in line with the work of Kántor et al. [45] who found that tree shading reduces PET around −9 K, during summertime in Pécs, Hungary. Findings of Berardi and Wang [8] support the strong decline in PET through building shade, with values of −17.5 K (10:00) and −14.1 K (14:00). Remarkably lower PET during the day inside of courtyards and east-west streets are consistent with the study by Taleghani et al. [84], who investigated different building arrangements.

The new buildings prevent ground-level surfaces from absorbing shortwave radiation. The buildings themselves absorb shortwave radiation and the associated increase in surface temperature enhances the outgoing longwave radiation. This mechanism largely explains the differences of the PET patterns during daytime and nighttime (Fig. 5a, 5b). In addition, heat accumulation is amplified as new buildings increase the roughness length and deflect or even block the wind flow. This enhances heat divergence and weakens the thermal mixing in the near-surface boundary layer.

Ketterer and Matzarakis [47] modelled urban re-planning in Stuttgart and discovered instantaneous PET to be around −10 K lower under trees compared to green areas and at least −25 K lower than over sealed surfaces. Johansson and Emmanuel [41] investigated PET in Colombo, Sri Lanka, and found the most comfortable conditions to be in narrow streets with tall buildings and the worst conditions to be in wide streets and open spaces without shade, which is also in line with the findings of this study.

4.2.3. Specific sites

We select both sites to highlight individual examples of direct and indirect urban development impacts. The *park site* is a location that remains unchanged itself, but the surrounding urban environment changes as new trees and buildings are added. In contrast, the *road site* is directly converted from an asphalted road to a short grass spot with nearby trees. In both cases, the changes lead to considerable changes in the energy balance, air temperature, PET, and surface temperature.

At the *park site* the shading by nearby trees in the future scenario reduces the latent heat flux and net shortwave radiation. The newly constructed buildings that surround the park enhance the outgoing longwave radiation increasing the longwave budget. The peak values of net longwave radiation correspond to the lows of net shortwave radiation and the latent heat flux. This is due to the nearby trees that receive more radiant energy at treetop height and thus emit more longwave radiation toward the *park site*. The absence (current) and presence (future) of buildings and related longwave radiation changes most likely account for the positive air temperature and PET differences (nighttime) of the *park site*. Besides the dominating impact of tree shading, leaf crowns reduce wind velocities and block/hinder vertical mixing, amplifying near-surface heat accumulation. New buildings also impact circulation patterns by considerably reducing wind speeds within the centre of the model domain.

The conversion of the *road site* increases the albedo and heat capacity and reduced the heat storage. These changes might explain the strong decrease in shortwave radiation, surface temperature, and the decline in ground heat flux. Moreover, it might explain the pronounced shift from sensible to latent heat flux. Longwave net radiation increases even though adjacent sealed surfaces as well as five residential buildings in the north disappear (distance: approx. 10 – 50 m). Possibly, it is an interplay of trees and a distant influence of the newly emerged centre. Shading due to more trees accounts for the net shortwave radiation drop during the day, which might also be reflected in the PET, as mean radiant temperature declines substantially. Conclusively, the conversion from sealed to vegetated surface, the removal of nearby buildings, the introduction of new trees can be considered responsible for lower air temperature and PET values of the *road site*.

5. Conclusion

In this study, we model the impacts of a planned urban development project (0.22 km^2) on the micro-meteorological conditions. PALM-4U resolves the thermal comfort and atmospheric motions at micro-scale (2 m), which allows to assess the small-scale impacts. The implications are analysed for two distinct urban configurations - the current scenario before the reconstruction (2018) and the future scenario after completion (2025) - for one of the hottest summer days with clear-sky conditions during a heatwave. In particular, the changes in air temperature, outdoor thermal comfort, using physiologically equivalent temperature (PET), and the diurnal energy balance of specific locations are considered.

Both during the day and the night, mean near-surface air temperature increases within the newly constructed residential area, with more pronounced warming during daytime. In contrast, the air temperature decreases over areas, where building areas, bare soil, and sealed surfaces are converted into green spaces with extensive vegetation. The PET shows higher variations and amplitudes. During the day, a spatially heterogeneous pattern of low and high thermal exposure is observed, determined by changes in incoming radiation. At night, PET increases in the centre and is consistent with the findings for near-surface air temperature. Despite the large-scale development, surrounding areas are barely affected by changes. This indicates the limited area of influence that the development project has on adjacent non-modified structures.

The microclimatic changes are most likely due to the reconstruction of buildings, which represent by far the largest structural changes. Buildings lead to changes in the energy balance, heat trapping, and lower horizontal wind velocities. The PET is highly sensitive to shading from new buildings and trees, lowering mean radiant temperature and thus the PET, primarily during daytime periods with low sun angles. The cooling impact of vegetation occurs at very small-scale. However, the impact of the specific building configuration examined in this study appears to be dominant in terms of microclimatic changes. In conclusion, the effect of adaptation measures designed to increase the cooling effects is reduced by the pronounced impact of new buildings.

We conclude that modelling real urban development projects at micro-scale can help to improve our understanding of distinct small-

scale changes, e.g. impact of buildings properties, street trees, and surface cover changes. More importantly, it enables the assessment of interrelated meteorological processes that govern the microclimate within an urban environment. During the planning of large development projects, such simulations should have greater importance. By implementing feasible urban planning and mitigation strategies into the study design, further investigations could help to minimise heat stress during summer. Technical progress towards more computational power reduces trade-offs between model domain size and fine resolution and supports similar study designs in the future.

The main future challenge is to understand implications of an urban development projects in its entirety and nonetheless scrutinise all the micro-scale processes that contribute to it. In the face of a globally growing urban population, implications of structural urban changes on surface-atmosphere interactions will remain an issue of paramount importance. This study can provide a framework for further investigation and can contribute to urban planning and urban adaptation to heatwaves.

CRediT authorship contribution statement

Julian Anders: Conceptualization, Formal analysis, Investigation, Methodology, Software, Validation, Visualization, Writing – original draft, Writing – review & editing. **Sebastian Schubert:** Conceptualization, Funding acquisition, Methodology, Project administration, Supervision, Writing – review & editing. **Tobias Sauter:** Resources, Supervision, Writing – review & editing. **Siiri Tunn:** Writing – review & editing. **Christoph Schneider:** Supervision, Writing – review & editing. **Mohamed Salim:** Conceptualization, Methodology, Supervision, Writing – review & editing.

Declaration of competing interest

The authors declare the following financial interests/personal relationships which may be considered as potential competing interests:

Julian Anders, Sebastian Schubert, Siiri Tunn, Mohamed Salim reports financial support was provided by Federal Ministry of Education and Research Berlin Office.

Data availability

Data will be made available on request.

Acknowledgements

Julian Anders was supported by the Federal German Ministry of Education and Research (BMBF) grant 01UR2021B, Sebastian Schubert was partly supported by BMBF grant 033W107C, Mohamed Salim was supported by Module A of the BMBF -Programme [UC]2: MOSAIK-2 - further development of PALM-4U (grant 01LP1911E), and Siiri Tunn was supported by BMBF grant 01UR2021B. Additionally, we acknowledge the funding received from Modul B of the BMBF-Programme [UC]2: 3DO+M - evaluation and scientific application of PALM-4U (project number: 01LP1912) to cover the publication fees associated with this work.

Appendix A. Methods - evaluation of input forcing data

We evaluated the COSMO Forcing data with local air temperature data measured at DWD stations (Fig. B.10). Therefore, we selected four measuring stations located at a maximum distance of 40 km from the study site. We chose rural measuring sites, as the COSMO model lacks urban parameterisation, which might cause large differences over urban environments. Time series analysis was carried out based on linear regression, Pearson correlation, bias, mean-absolute-error (MAE), and root-mean-squared-error (RMSE).

Appendix B. Results - evaluation of input forcing data

The outcome of the forcing data evaluation is depicted in Fig. B.11. Overall, the three-month time series of COSMO model data matches the local measuring station data very well. All four data pairs have a correlation of 0.99, a bias smaller than ± 0.7 K, an MAE below 0.8 K, and an RMSE around 1 K. Thereby, all correlations are statistically significant (p-value < 0.01), and a Shapiro-Wilk test indicates that all datasets are normally distributed.

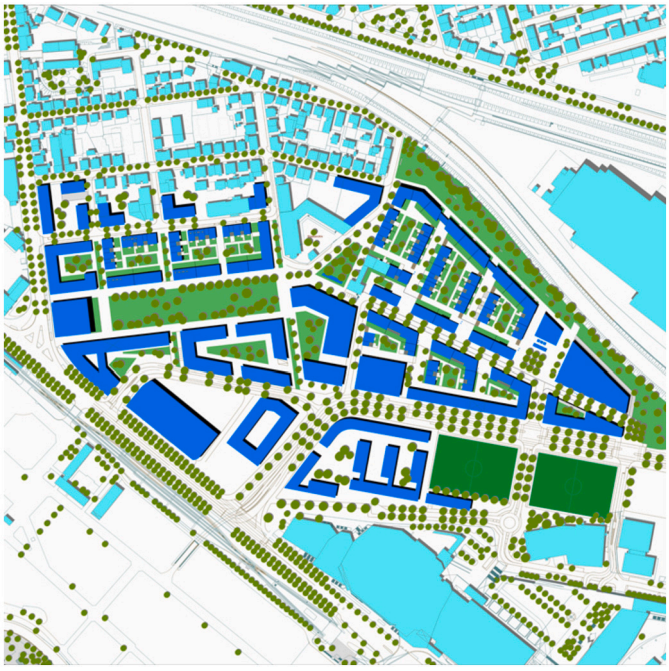

Fig. B.8. Commercial figure of the construction plans for the urban development site Neckarpark that constitutes the basis for implementing the future scenario. Source: https://www.stuttgart-meine-stadt.de/stadtentwicklung/neckarpark/.

Fig. B.9. Differences between the assigned land use in the official development plans of the Stuttgart City Planning Office (left) and the adapted plans with inserted building shapes, paths, single trees, and green patches (right). The classification corresponds to the assigned main functionality of the areas.

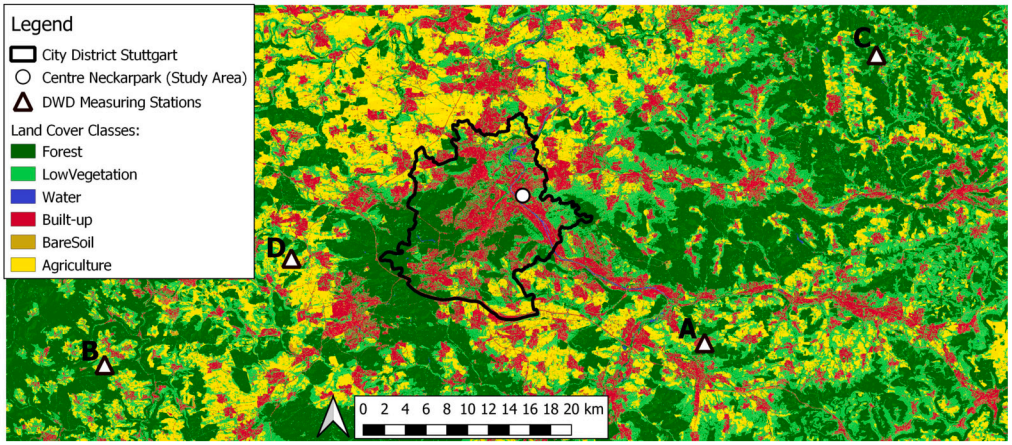

Fig. B.10. Land cover map with local DWD stations selected for evaluation of COSMO forcing data. Measuring stations are located in Notzingen (A), Neubulach-Oberhaugstett (B), Kaiserbach-Cronhütte (C), Renningen-Ihinger Hof (D). All stations are sited in rural areas with a maximum distance of 40 km to the centre of the study area Neckarpark.

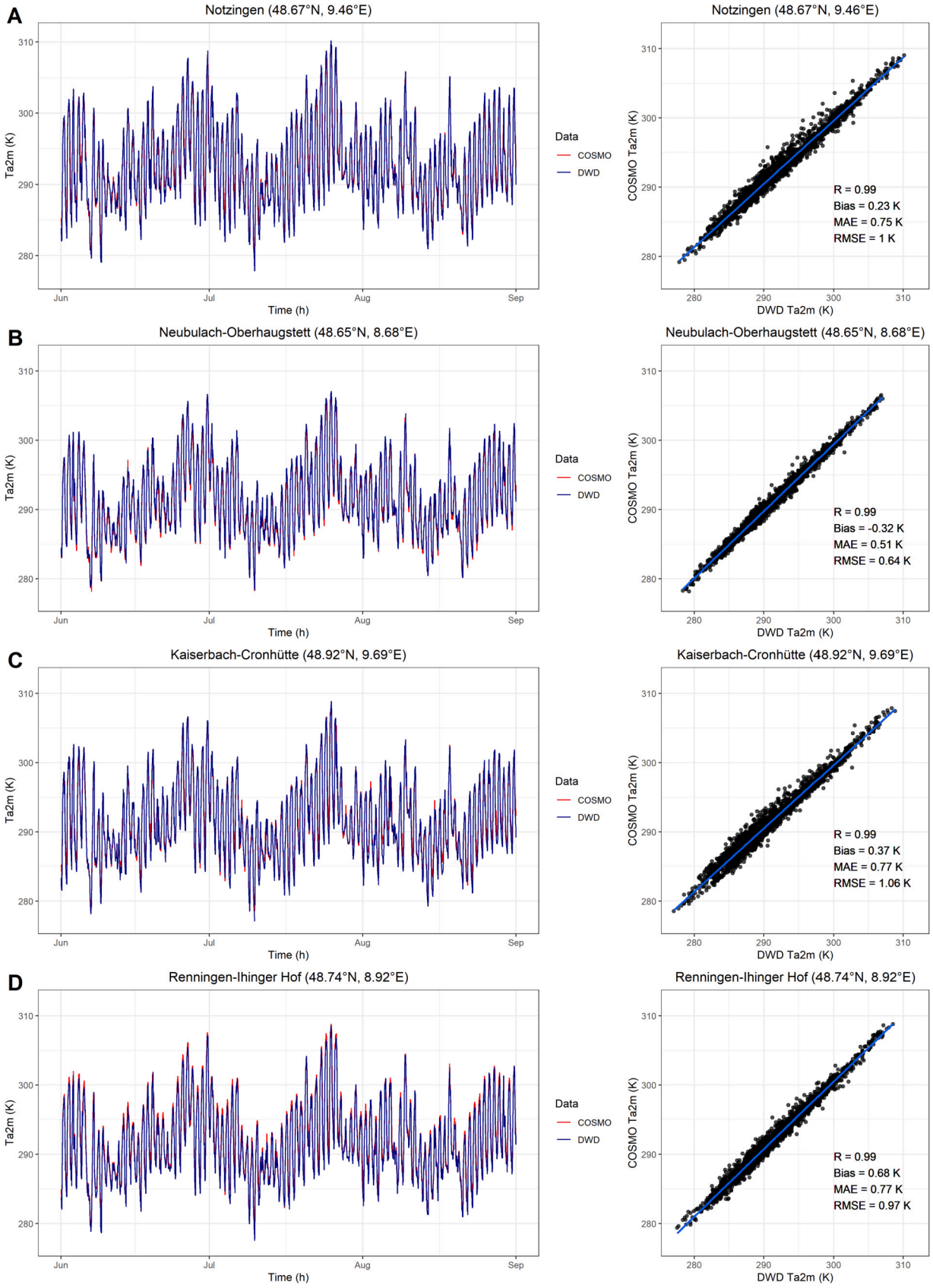

Fig. B.11. Evaluation of COSMO forcing data by investigating air temperature (2 m) and comparing it to four local measuring stations of the German Meteorological Service (DWD). Three-month time series (left) and linear regressions (right) are examined at the locations of Notzingen (A), Neubulach-Oberhaugstett (B), Kaiserbach-Cronhütte (C), and Renningen-Ihinger Hof (D).

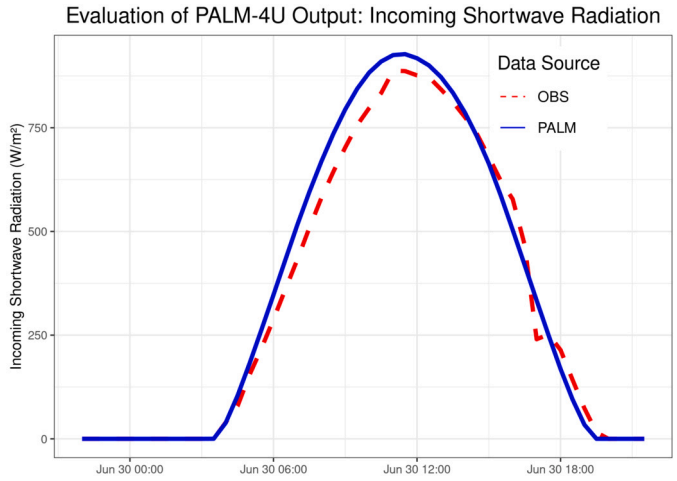

Fig. B.12. Incoming shortwave radiation for the *PALM* run and the local measuring data *OBS*. The measuring station is the on the roof of the fire station, which corresponds to Point *M* in Fig. 2.

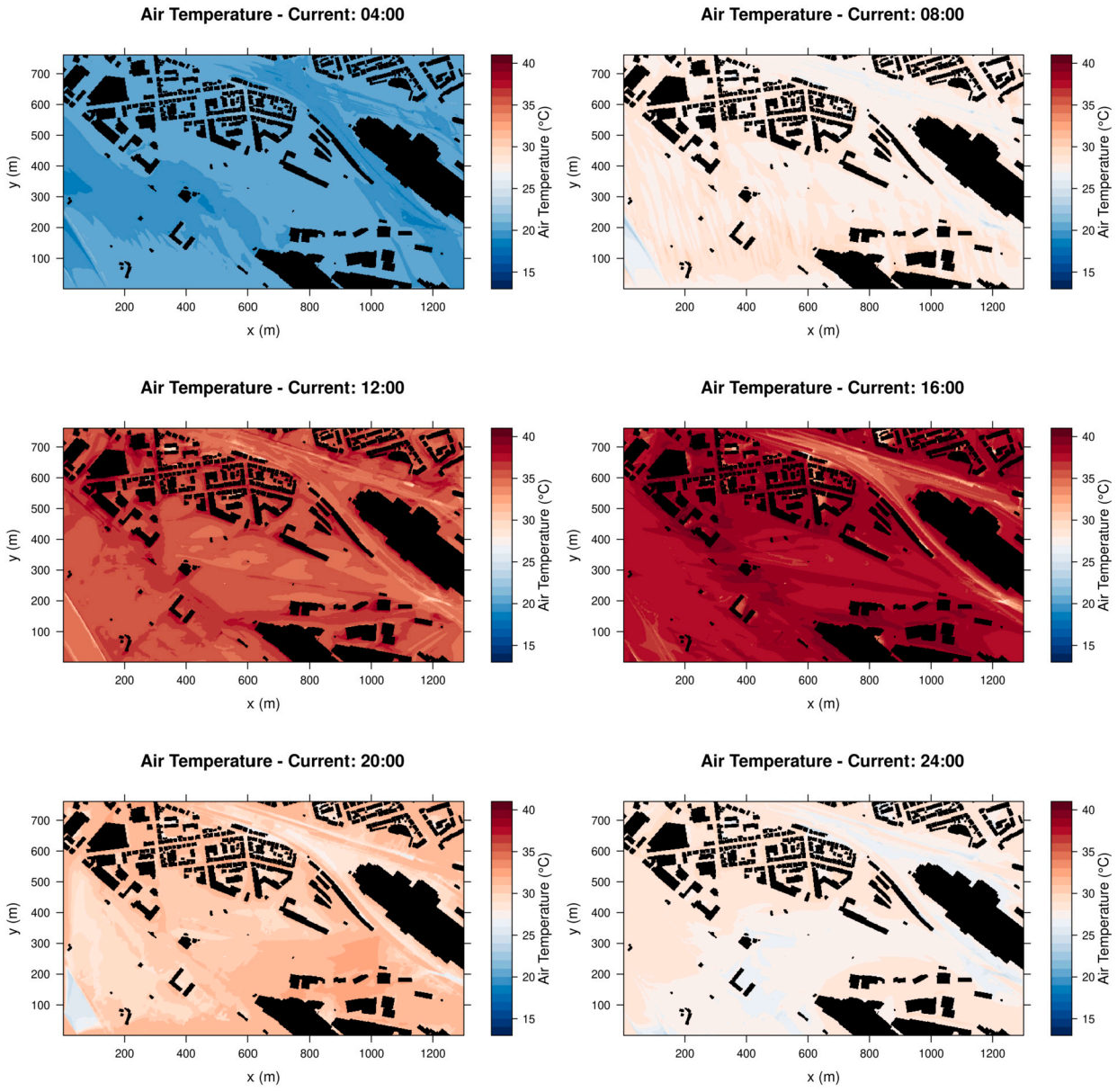

Fig. B.13. PALM-4U model output for the current scenario showing the diurnal cycle of the near-surface air temperature. Absolute temperature values are shown for the state at 04:00, 08:00, 12:00, 16:00, 20:00, and 24:00 UTC. The black objects are buildings in at least one of the two scenarios.

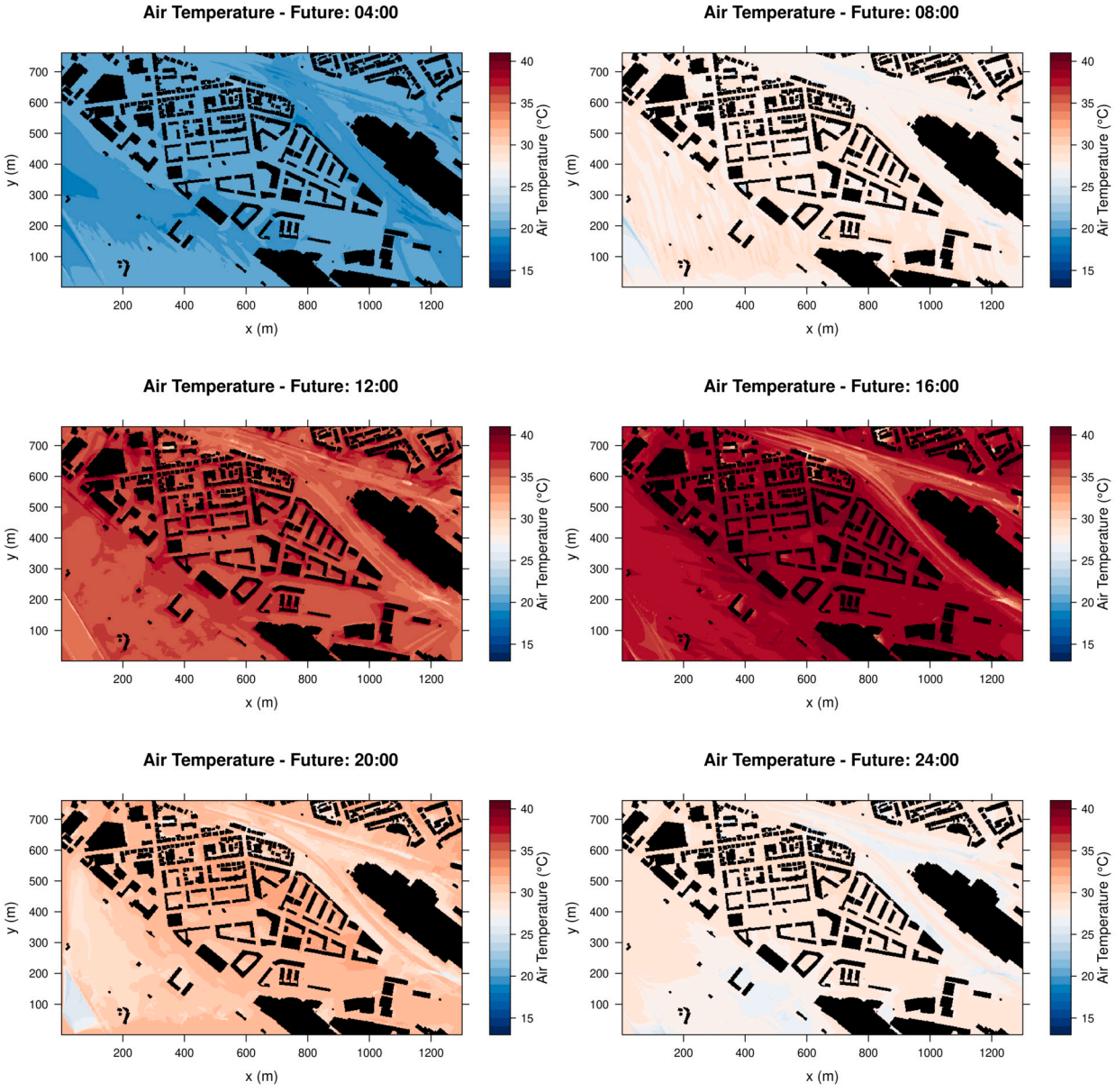

Fig. B.14. PALM-4U model output for the future scenario showing the diurnal cycle of the near-surface air temperature. Absolute temperature values are shown for the state at 04:00, 08:00, 12:00, 16:00, 20:00, and 24:00 UTC. The black objects are buildings in at least one of the two scenarios.

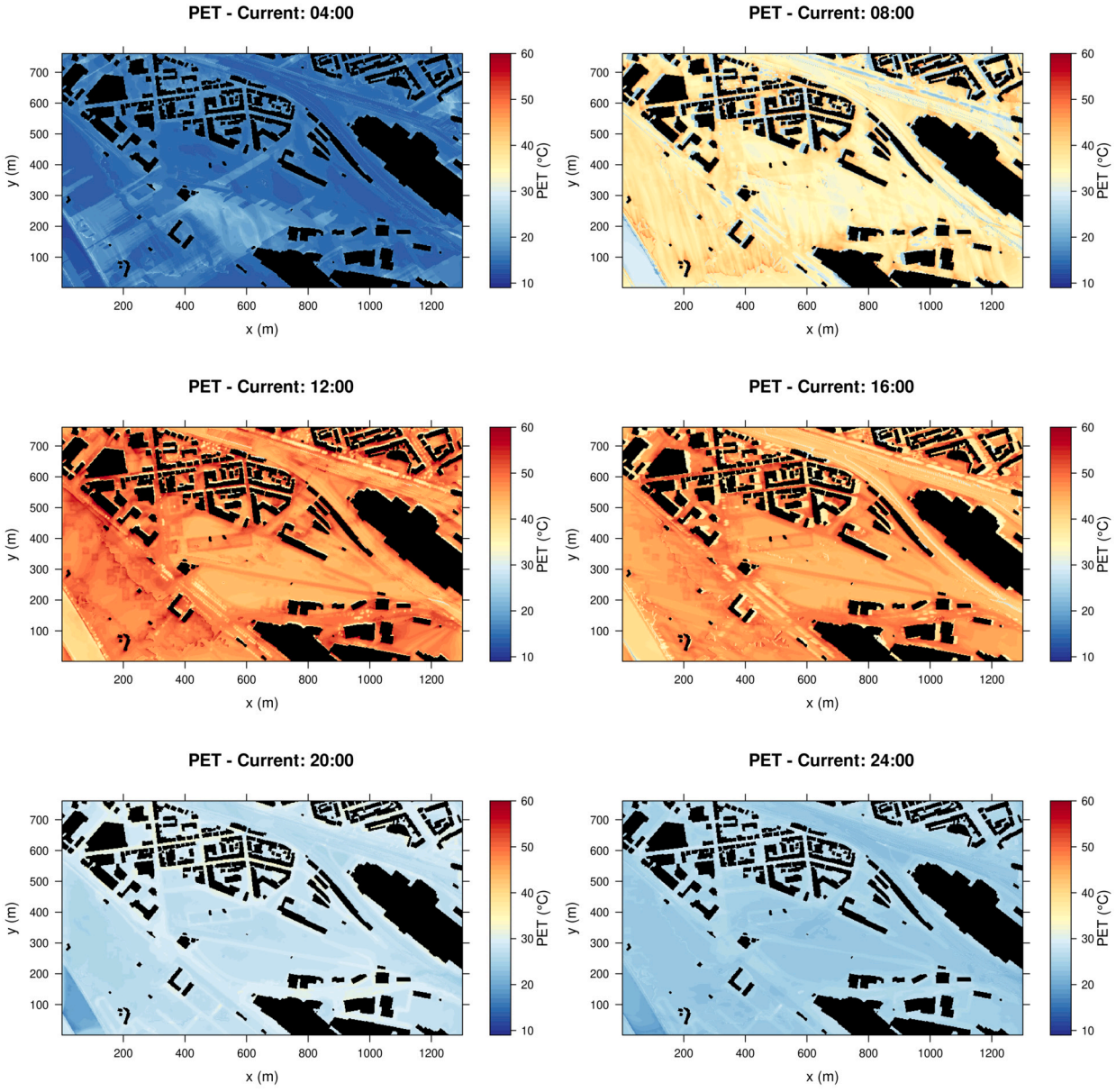

Fig. B.15. PALM-4U model output for the current scenario showing the diurnal cycle of the PET. Absolute PET values are shown for the state at 04:00, 08:00, 12:00, 16:00, 20:00, and 24:00 UTC. The black objects are buildings in at least one of the two scenarios.

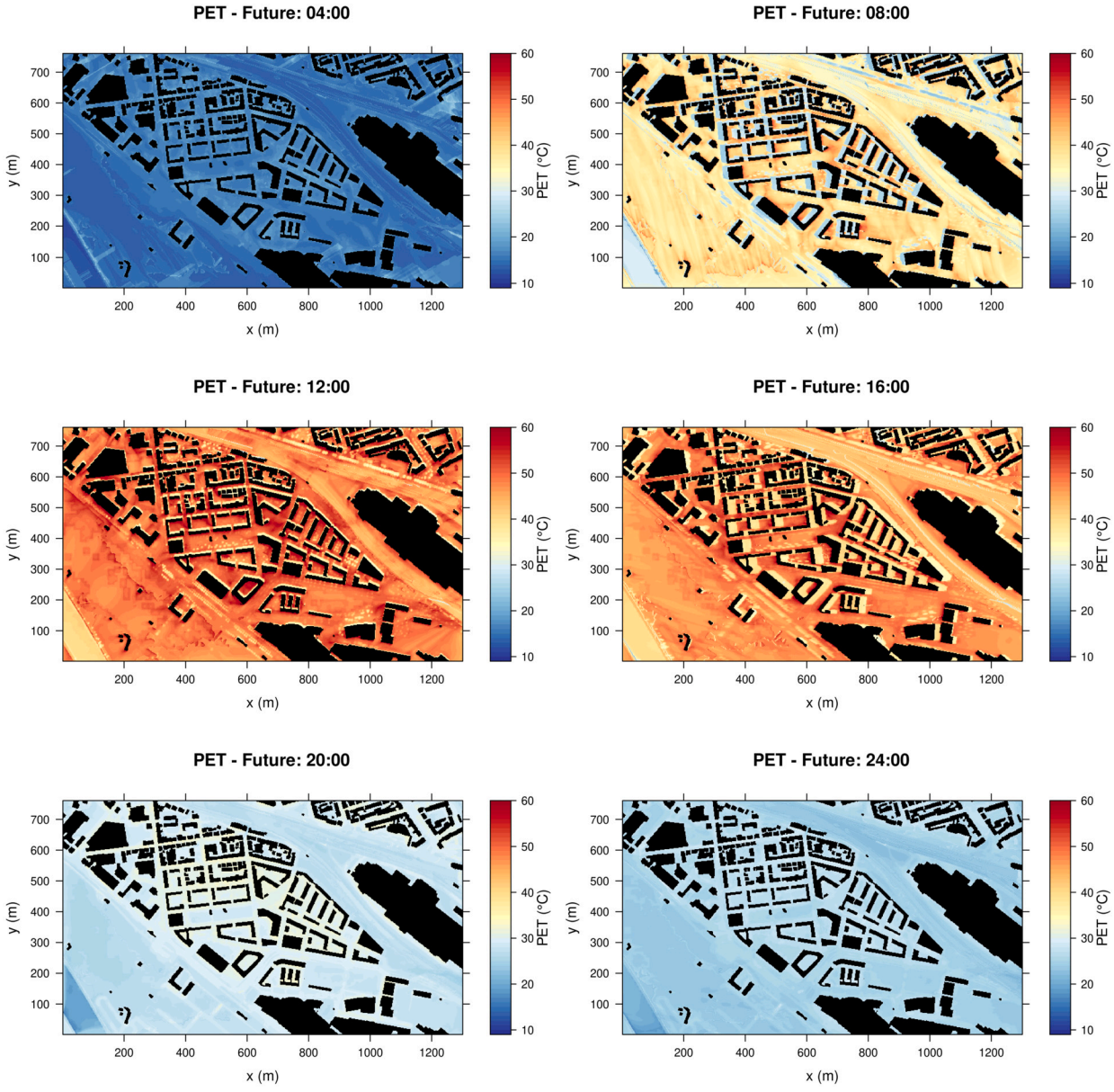

Fig. B.16. PALM-4U model output for the future scenario showing the diurnal cycle of the PET. Absolute PET values are shown for the state at 04:00, 08:00, 12:00, 16:00, 20:00, and 24:00 UTC. The black objects are buildings in at least one of the two scenarios.

References

[1] F. Ali-Toudert, H. Mayer, Numerical study on the effects of aspect ratio and orientation of an urban street canyon on outdoor thermal comfort in hot and dry climate, Build. Environ. 41 (2006) 94–108, https://doi.org/10.1016/j.buildenv.2005.01.013.

[2] Amt für Stadtplanung und Stadterneuerung, Stadtquartier neckarpark, https://www.stuttgart-meine-stadt.de/stadtentwicklung/neckarpark/, 2020.

[3] Amt für Stadtplanung und Wohnen, Neckarpark: urban, lebenswert und nachhaltig, https://www.stuttgart-meine-stadt.de/file/5e68a99fc9e30776836c8322, 2019.

[4] M. Baldauf, C. Gebhardt, S. Theis, B. Ritter, C. Schraff, Beschreibung des operationellen kürzestfristvorhersagemodells cosmo-d2 und cosmo-d2-eps und seiner ausgabe in datenbanken des dwd, Deutscher Wetterdienst, 2018, pp. 1–115.

[5] G. Battista, E. Carnielo, R. De Lieto Vollaro, Thermal impact of a redeveloped area on localized urban microclimate: a case study in Rome, Energy Build. 133 (2016) 446–454, https://doi.org/10.1016/j.enbuild.2016.10.004.

[6] J. Baumueller, U. Reuter, Stadtklimatische aspekte am beispiel stuttgart, Geowissenschaften (1996) 229–232.

[7] M. Belda, J. Resler, J. Geletič, P. Krč, B. Maronga, M. Sühring, M. Kurppa, F. Kanani-Sühring, V. Fuka, K. Eben, N. Benešová, M. Auvinen, Sensitivity analysis of the PALM model system 6.0 in the urban environment, Geosci. Model Dev. 14 (2021) 4443–4464, https://doi.org/10.5194/gmd-14-4443-2021.

[8] U. Berardi, Y. Wang, The effect of a denser city over the urban microclimate: the case of Toronto, Sustainability 8 (2016) 822, https://doi.org/10.3390/su8080822.

[9] J. Birkmann, M. Garschagen, F. Kraas, N. Quang, Adaptive urban governance: new challenges for the second generation of urban adaptation strategies to climate change, Sustain. Sci. 5 (2010) 185–206, https://doi.org/10.1007/s11625-010-0111-3.

[10] B. Blocken, Les over rans in building simulation for outdoor and indoor applications: a foregone conclusion?, Build. Simul. 11 (2018) 821–870, https://doi.org/10.1007/s12273-018-0459-3.

[11] M. Bruse, H. Fleer, Simulating surface–plant–air interactions inside urban environments with a three dimensional numerical model, Environ. Model. Softw. 13 (1998) 373–384, https://doi.org/10.1016/S1364-8152(98)00042-5.

[12] G. Büttner, CORINE Land Cover and Land Cover Change Products, Springer Netherlands, Dordrecht, 2014, pp. 55–74, https://doi.org/10.1007/978-94-007-7969-3_5.

[13] G. Büttner, G. Maucha, B. Kosztra, European validation of land cover changes in clc2006 project, in: EARSeL Symposium, Prague, 2011, pp. 336–351.

[14] T.N. Carlson, F.E. Boland, Analysis of urban-rural canopy using a surface heat flux/temperature model, J. Appl. Meteorol. 17 (1978) 998–1013, https://doi.org/10.1175/1520-0450(1978)017<0998:aourcu>2.0.co;2.

[15] J.G. Carter, G. Cavan, A. Connelly, S. Guy, J. Handley, A. Kazmierczak, Climate change and the city: building capacity for urban adaptation, Prog. Plann. 95 (2015) 1–66, https://doi.org/10.1016/j.progress.2013.08.001.

[16] S. Chatterjee, A. Khan, A. Dinda, S. Mithun, R. Khatun, H. Akbari, H. Kusaka, C. Mitra, S.S. Bhatti, Q. van Doan, Y. Wang, Simulating micro-scale thermal interactions in different building environments for mitigating urban heat islands, Sci. Total Environ. 663 (2019) 610–631, https://doi.org/10.1016/j.scitotenv.2019.01.299.

[17] S.A. Clough, M.W. Shephard, E.J. Mlawer, J.S. Delamere, M.J. Iacono, K. Cady-Pereira, S. Boukabara, P.D. Brown, Atmospheric radiative transfer modeling: a summary of the aer codes, J. Quant. Spectrosc. Radiat. Transf. 91 (2005) 233–244, https://doi.org/10.1016/j.jqsrt.2004.05.058.

[18] Copernicus Land Monitoring Service, Corine land cover 2012 100 m, https://land.copernicus.eu/pan-european/corine-land-cover/, 2017.

[19] J. Cortekar, L. Willen, B. Büter, M. Winkler, R. Hölsgens, C. Burmeister, S. Dankwart-Kammoun, A. Kriuger, B. Steuri, Basics for the operationalization of the new urban climate model palm-4u, Clim. Serv. 20 (2020) 100193, https://doi.org/10.1016/j.cliser.2020.100193.

[20] G. Doms, M. Baldauf, Cosmo-model version 5.00: a description of the nonhydrostatic regional cosmo-model - part I: dynamics and numerics, https://doi.org/10.5676/DWD_pub/nwv/cosmo-doc_5.00_I.

[21] G. Doms, J. Förstner, E. Heise, H.J. Herzog, D. Mironov, M. Raschendorfer, T. Reinhardt, B. Ritter, R. Schrodin, J.P. Schulz, G. Vogel, A description of the nonhydrostatic regional cosmo model - part ii: physical parameterization, http://www2.cosmo-model.org/content/model/documentation/core/cosmo_physics_4.20.pdf, 2011.

[22] DWD, Yearbook 2019 of the deutscher wetterdienst, 2020, pp. 1–72, https://www.dwd.de/EN/ourservices/annual_reports_dwd/annual_reports_pdf/annual_report_2019.pdf?__blob=publicationFile&v=2.

[23] R. Emmanuel, H.J. Fernando, Urban heat islands in humid and arid climates: role of urban form and thermal properties in Colombo, Sri Lanka and Phoenix, USA, Clim. Res. 34 (2007) 241–251, https://doi.org/10.3354/cr00694.

[24] J. Estima, M. Painho, Investigating the Potential of OpenStreetMap for Land Use/Land Cover Production: A Case Study for Continental Portugal, Springer International Publishing, 2015, pp. 273–293, https://doi.org/10.1007/978-3-319-14280-7_14.

[25] T. Foken, Micrometeorology, 2nd ed. 2017 ed., Springer Berlin Heidelberg, Berlin, Heidelberg and S.L., 2017, https://doi.org/10.1007/978-3-642-25440-6.

[26] D. Fröhlich, A. Matzarakis, Calculating human thermal comfort and thermal stress in the PALM model system 6.0, Geosci. Model Dev. 13 (2020) 3055–3065, https://doi.org/10.5194/gmd-13-3055-2020.

[27] B. Früh, P. Becker, T. Deutschländer, J.D. Hessel, M. Kossmann, I. Mieskes, J. Namyslo, M. Roos, U. Sievers, T. Steigerwald, H. Turau, U. Wienert, Estimation of climate-change impacts on the urban heat load using an urban climate model and regional climate projections, J. Appl. Meteorol. Climatol. 50 (2011) 167–184, https://doi.org/10.1175/2010JAMC2377.1.

[28] E. Gago, J. Roldan, R. Pacheco-Torres, J. Ordóñez, The city and urban heat islands: a review of strategies to mitigate adverse effects, Renew. Sustain. Energy Rev. 25 (2013) 749–758, https://doi.org/10.1016/j.rser.2013.05.057.

[29] K.F. Gehrke, M. Sühring, B. Maronga, Modeling of land–surface interactions in the PALM model system 6.0: land surface model description, first evaluation, and sensitivity to model parameters, Geosci. Model Dev. 14 (2021) 5307–5329, https://doi.org/10.5194/gmd-14-5307-2021.

[30] J. Geletič, M. Lehnert, P. Krč, J. Resler, E.S. Krayenhoff, High-resolution modelling of thermal exposure during a hot spell: a case study using palm-4u in Prague, Czech Republic, Atmosphere 12 (2021) 175, https://doi.org/10.3390/atmos12020175.

[31] J. Geletič, M. Lehnert, M. Jurek, Spatiotemporal variability of air temperature during a heat wave in real and modified landcover conditions: Prague and Brno (Czech Republic), Urban Clim. 31 (2020) 100588, https://doi.org/10.1016/j.uclim.2020.100588.

[32] D. Grawe, H.L. Thompson, J.A. Salmond, X.M. Cai, K.H. Schlünzen, Modelling the impact of urbanisation on regional climate in the greater London area, Int. J. Climatol. 33 (2013) 2388–2401, https://doi.org/10.1002/joc.3589.

[33] T. Gronemeier, K. Surm, F. Harms, B. Leitl, B. Maronga, S. Raasch, Evaluation of the dynamic core of the PALM model system 6.0 in a neutrally stratified urban environment: comparison between LES and wind-tunnel experiments, Geosci. Model Dev. 14 (2021) 3317–3333, https://doi.org/10.5194/gmd-14-3317-2021.

[34] G. Gross, Effects of different vegetation on temperature in an urban building environment. Micro-scale numerical experiments, Meteorol. Z. 21 (2012) 399–412, https://doi.org/10.1127/0941-2948/2012/0363.

[35] G. Hatvani-Kovacs, J. Bush, E. Sharifi, J. Boland, Policy recommendations to increase urban heat stress resilience, Urban Clim. 25 (2018) 51–63, https://doi.org/10.1016/j.uclim.2018.05.001.

[36] W. Heldens, C. Burmeister, F. Kanani-Sühring, B. Maronga, D. Pavlik, M. Sühring, J. Zeidler, T. Esch, Geospatial input data for the palm model system 6.0: model requirements, data sources, and processing, Geosci. Model Dev. (2020), https://doi.org/10.5194/gmd-2019-355.

[37] M.P. Heris, A. Middel, B. Muller, Impacts of form and design policies on urban microclimate: assessment of zoning and design guideline choices in urban redevelopment projects, Landsc. Urban Plan. 202 (2020) 103870, https://doi.org/10.1016/j.landurbplan.2020.103870.

[38] J. Herrmann, A. Matzarakis, Mean radiant temperature in idealised urban canyons–examples from Freiburg, Germany, Int. J. Biometeorol. 56 (2012) 199–203, https://doi.org/10.1007/s00484-010-0394-1.

[39] P. Höppe, The physiological equivalent temperature—a universal index for the biometeorological assessment of the thermal environment, Int. J. Biometeorol. (1999) 71–75.

[40] IPCC, Urban areas, Chapter 8, in: AR5 Climate Change 2014: Impacts, Adaptation, and Vulnerability, 2014, pp. 535–612, https://www.ipcc.ch/site/assets/uploads/2018/02/WGIIAR5-Chap8_FINAL.pdf.

[41] E. Johansson, R. Emmanuel, The influence of urban design on outdoor thermal comfort in the hot, Humid city of Colombo, Sri Lanka, Int. J. Biometeorol. 51 (2006) 119–133, https://doi.org/10.1007/s00484-006-0047-6.

[42] D.P. Johnson, J.S. Wilson, The socio-spatial dynamics of extreme urban heat events: the case of heat-related deaths in Philadelphia, Appl. Geogr. 29 (2009) 419–434, https://doi.org/10.1016/j.apgeog.2008.11.004.

[43] E. Kadasch, M. Sühring, T. Gronemeier, S. Raasch, Mesoscale nesting interface of the palm model system 6.0, Geosci. Model Dev. 14 (2021) 5435–5465, https://doi.org/10.5194/gmd-14-5435-2021.

[44] F. Kanani, K. Träumner, B. Ruck, S. Raasch, What determines the differences found in forest edge flow between physical models and atmospheric measurements? – an les study, Meteorol. Z. 23 (2014) 33–49, https://doi.org/10.1127/0941-2948/2014/0542.

[45] N. Kántor, L. Chen, C.V. Gál, Human-biometeorological significance of shading in urban public spaces—summertime measurements in Pécs, Hungary, Landsc. Urban Plan. 170 (2018) 241–255, https://doi.org/10.1016/j.landurbplan.2017.09.030.

[46] S. Karttunen, M. Kurppa, M. Auvinen, A. Hellsten, L. Järvi, Large-eddy simulation of the optimal street-tree layout for pedestrian-level aerosol particle concentrations – a case study from a city-boulevard, Atmos. Environ. X 6 (2020) 100073, https://doi.org/10.1016/j.aeaoa.2020.100073.

[47] C. Ketterer, A. Matzarakis, Human-biometeorological assessment of heat stress reduction by replanning measures in Stuttgart, Germany, Landsc. Urban Plan. 122 (2014) 78–88, https://doi.org/10.1016/j.landurbplan.2013.11.003.

[48] C. Ketterer, A. Matzarakis, Human-biometeorological assessment of the urban heat island in a city with complex topography – the case of Stuttgart, Germany, Urban Clim. 10 (2014) 573–584, https://doi.org/10.1016/j.uclim.2014.01.003.

[49] B. Khan, S. Banzhaf, E.C. Chan, R. Forkel, F. Kanani-Sühring, K. Ketelsen, M. Kurppa, B. Maronga, M. Mauder, S. Raasch, E. Russo, M. Schaap, M. Sühring, Development of an atmospheric chemistry model coupled to the PALM model system 6.0: implementation and first applications, Geosci. Model Dev. 14 (2021) 1171–1193, https://doi.org/10.5194/gmd-14-1171-2021.

[50] S.M. Khan, R.W. Simpson, Effect of a heat island on the meteorology of a complex urban airshed, Bound.-Layer Meteorol. (2001) 487–506.
[51] F. Koch, L. Bilke, C. Helbig, U. Schlink, Compact or cool? The impact of brownfield redevelopment on inner-city micro climate, Sustain. Cities Soc. 38 (2018) 31–41, https://doi.org/10.1016/j.scs.2017.11.021.
[52] M. Kottek, J. Grieser, C. Beck, B. Rudolf, F. Rubel, World map of the Köppen-Geiger climate classification updated, Meteorol. Z. 15 (2006) 259–263, https://doi.org/10.1127/0941-2948/2006/0130.
[53] P. Krč, J. Resler, M. Sühring, S. Schubert, M.H. Salim, V. Fuka, Radiative transfer model 3.0 integrated into the PALM model system 6.0, Geosci. Model Dev. 14 (2021) 3095–3120, https://doi.org/10.5194/gmd-14-3095-2021.
[54] M. Krutova, M. Bakhoday-Paskyabi, J. Reuder, F.G. Nielsen, Self-nested large-eddy simulations in palm model system v21.10 for offshore wind prediction under different atmospheric stability conditions, Geosci. Model Dev. Discuss. 2022 (2022) 1–18, https://doi.org/10.5194/gmd-2022-256.
[55] W. Leal Filho, L. Echevarria Icaza, V.O. Emanche, A. Quasem Al-Amin, An evidence-based review of impacts, strategies and tools to mitigate urban heat islands, Int. J. Environ. Res. Public Health 14 (2017) 1600.
[56] M.O. Letzel, M. Krane, S. Raasch, High resolution urban large-eddy simulation studies from street canyon to neighbourhood scale, Atmos. Environ. 42 (2008) 8770–8784, https://doi.org/10.1016/j.atmosenv.2008.08.001.
[57] B. Maronga, S. Banzhaf, C. Burmeister, T. Esch, R. Forkel, D. Fröhlich, V. Fuka, K.F. Gehrke, J. Geletič, S. Giersch, T. Gronemeier, G. Groß, W. Heldens, A. Hellsten, F. Hoffmann, A. Inagaki, E. Kadasch, F. Kanani-Sühring, K. Ketelsen, B.A. Khan, C. Knigge, H. Knoop, P. Krč, M. Kurppa, H. Maamari, A. Matzarakis, M. Mauder, M. Pallasch, D. Pavlik, J. Pfafferott, J. Resler, S. Rissmann, E. Russo, M. Salim, M. Schrempf, J. Schwenkel, G. Seckmeyer, S. Schubert, M. Sühring, R. Tils, L. Vollmer, S. Ward, B. Witha, H. Wurps, J. Zeidler, S. Raasch, Overview of the palm model system 6.0, Geosci. Model Dev. 13 (2020) 1335–1372, https://doi.org/10.5194/gmd-13-1335-2020.
[58] B. Maronga, G. Gross, S. Raasch, S. Banzhaf, R. Forkel, W. Heldens, F. Kanani-Sühring, A. Matzarakis, M. Mauder, D. Pavlik, J. Pfafferott, S. Schubert, G. Seckmeyer, H. Sieker, K. Winderlich, Development of a new urban climate model based on the model palm – project overview, planned work, and first achievements, Meteorol. Z. 28 (2019) 105–119, https://doi.org/10.1127/metz/2019/0909.
[59] B. Maronga, M. Gryschka, R. Heinze, F. Hoffmann, F. Kanani-Sühring, M. Keck, K. Ketelsen, M.O. Letzel, M. Sühring, S. Raasch, The parallelized large-eddy simulation model (palm) version 4.0 for atmospheric and oceanic flows: model formulation, recent developments, and future perspectives, Geosci. Model Dev. 8 (2015) 2515–2551, https://doi.org/10.5194/gmd-8-2515-2015.
[60] A. Matzarakis, P.T. Nastos, Human-biometeorological assessment of heat waves in Athens, Theor. Appl. Climatol. 105 (2011) 99–106, https://doi.org/10.1007/s00704-010-0379-3.
[61] T.R. Oke, The urban energy balance, Prog. Phys. Geogr., Earth Environ. 12 (1988) 471–508, https://doi.org/10.1177/030913338801200401.
[62] T.R. Oke, The micrometeorology of the urban forest, Philos. Trans. R. Soc. Lond. B, Biol. Sci. 324 (1989) 335–349, https://doi.org/10.1098/rstb.1989.0051.
[63] T.R. Oke, B.D. Kalanda, D.G. Steyn, Parameterization of heat storage in urban areas, Urban Ecol. 5 (1981) 45–54, https://doi.org/10.1016/0304-4009(81)90020-6.
[64] T.R. Oke, G. Mills, A. Christen, J.A. Voogt, Urban Climates, Cambridge University Press, 2017, https://doi.org/10.1017/9781139016476.
[65] I. Orlanski, A rational subdivision of scales for atmospheric processes, Bull. Am. Meteorol. Soc. (1975) 527–530.
[66] B. Paas, T. Zimmermann, O. Klemm, Analysis of a turbulent wind field in a street canyon: good agreement between les model results and data from a mobile platform, Meteorol. Z. (2020), https://doi.org/10.1127/metz/2020/1006.
[67] S.B. Park, J.J. Baik, B.S. Han, Large-eddy simulation of turbulent flow in a densely built-up urban area, Environ. Fluid Mech. 15 (2015) 235–250, https://doi.org/10.1007/s10652-013-9306-3.
[68] S.B. Park, J.J. Baik, S.H. Lee, Impacts of mesoscale wind on turbulent flow and ventilation in a densely built-up urban area, J. Appl. Meteorol. Climatol. 54 (2015) 811–824, https://doi.org/10.1175/jamc-d-14-0044.1.
[69] J. Pfafferott, S. Rißmann, M. Sühring, F. Kanani-Sühring, B. Maronga, Building indoor model in PALM-4u: indoor climate, energy demand, and the interaction between buildings and the urban microclimate, Geosci. Model Dev. 14 (2021) 3511–3519, https://doi.org/10.5194/gmd-14-3511-2021.
[70] R. Priyadarsini, W.N. Hien, C.K.W. David, Microclimatic modeling of the urban thermal environment of Singapore to mitigate urban heat island, Sol. Energy 82 (2008) 727–745.
[71] S. Raasch, M. Schröter, Palm - a large-eddy simulation model performing on massively parallel computers, Meteorol. Z. 10 (2001) 363–372, https://doi.org/10.1127/0941-2948/2001/0010-0363.
[72] J. Resler, K. Eben, J. Geletič, P. Krč, M. Rosecký, M. Sühring, M. Belda, V. Fuka, T. Halenka, P. Huszár, J. Karlický, N. Benešová, J. Ďoubalová, K. Honzáková, J. Keder, Š. Nápravníková, O. Vlček, Validation of the PALM model system 6.0 in a real urban environment: a case study in Dejvice, Prague, the Czech Republic, Geosci. Model Dev. 14 (2021) 4797–4842, https://doi.org/10.5194/gmd-14-4797-2021.
[73] J. Resler, P. Krč, M. Belda, P. Juruš, N. Benešová, J. Lopata, O. Vlček, D. Damašková, K. Eben, P. Derbek, B. Maronga, F. Kanani-Sühring, PALM-USM v1.0: a new urban surface model integrated into the PALM large-eddy simulation model, Geosci. Model Dev. 10 (2017) 3635–3659, https://doi.org/10.5194/gmd-10-3635-2017.
[74] K.D. Ridder, D. Lauwaet, B. Maiheu, Urbclim – a fast urban boundary layer climate model, Urban Clim. 12 (2015) 21–48, https://doi.org/10.1016/j.uclim.2015.01.001.
[75] M.W. Rotach, R. Vogt, C. Bernhofer, E. Batchvarova, A. Christen, A. Clappier, B. Feddersen, S.E. Gryning, G. Martucci, H. Mayer, V. Mitev, T.R. Oke, E. Parlow, H. Richner, M. Roth, Y.A. Roulet, D. Ruffieux, J.A. Salmond, M. Schatzmann, J.A. Voogt, Bubble – an urban boundary layer meteorology project, Theor. Appl. Climatol. 81 (2005) 231–261, https://doi.org/10.1007/s00704-004-0117-9.
[76] H.S. Salim, S. Schubert, B. Maronga, C. Schneider, M.F. Cidek, Introducing the urban climate model palm system 6.0, Int. J. Appl. Energy Syst. 2 (1) (2020) 15–18.
[77] M.H. Salim, K.H. Schlünzen, D. Grawe, M. Boettcher, A.M.U. Gierisch, B.H. Fock, The microscale obstacle-resolving meteorological model mitras v2.0: model theory, Geosci. Model Dev. 11 (2018) 3427–3445, https://doi.org/10.5194/gmd-11-3427-2018.
[78] M.H. Salim, S. Schubert, J. Resler, P. Krč, B. Maronga, F. Kanani-Sühring, M. Sühring, C. Schneider, Importance of radiative transfer processes in urban climate models: a study based on the PALM 6.0 model system, Geosci. Model Dev. 15 (2022) 145–171, https://doi.org/10.5194/gmd-15-145-2022.
[79] U. Schaettler, G. Doms, C. Schraff, Cosmo documentation part vii: user's guide: a description of the nonhydrostatic regional cosmo-model: Cosmo 5.06, http://www.cosmo-model.org/content/model/documentation/core/cosmo-io-guide.pdf, 2019.
[80] Stadtmessungsamt Stuttgart, Die digitale stadt stuttgart3d, https://www.stuttgart.de/medien/ibs/20190225_3DBroschuere_Gesamt_red.pdf, 2019.
[81] J. Steppeler, G. Doms, U. Schttler, H.W. Bitzer, A. Gassmann, U. Damrath, G. Gregoric, Meso-gamma scale forecasts using the nonhydrostatic model lm, Meteorol. Atmos. Phys. 82 (2003) 75–96, https://doi.org/10.1007/s00703-001-0592-9.
[82] I.D. Stewart, T.R. Oke, Local climate zones for urban temperature studies, Bull. Am. Meteorol. Soc. 93 (2012) 1879–1900, https://doi.org/10.1175/BAMS-D-11-00019.1.
[83] M.K. Svensson, Sky view factor analysis – implications for urban air temperature differences, Meteorol. Appl. 11 (1999) 201–211, https://doi.org/10.1017/S1350482704001288.
[84] M. Taleghani, L. Kleerekoper, M. Tenpierik, A. van den Dobbelsteen, Outdoor thermal comfort within five different urban forms in the Netherlands, Build. Environ. 83 (2015) 65–78, https://doi.org/10.1016/j.buildenv.2014.03.014.
[85] S. Thorsson, F. Lindberg, J. Björklund, B. Holmer, D. Rayner, Potential changes in outdoor thermal comfort conditions in Gothenburg, Sweden due to climate change: the influence of urban geometry, Int. J. Climatol. 31 (2011) 324–335, https://doi.org/10.1002/joc.2231.
[86] UN, World Urbanization Prospects: The 2018 Revision, United Nations, New York, 2019.
[87] J. Unger, Intra-urban relationship between surface geometry and urban heat island: review and new approach, Clim. Res. 27 (2004) 253–264.
[88] R. Vautard, Maarten van Aalst, O. Boucher, A. Drouin, K. Haustein, F. Kreienkamp, Geert Jan van Oldenborgh, F.E.L. Otto, A. Ribes, Y. Robin, M. Schneider, J.M. Soubeyroux, P. Stott, S.I. Seneviratne, M.M. Vogel, M. Wehner, Human contribution to the record-breaking June and July 2019 heatwaves in Western Europe, Environ. Res. Lett. (2020) 1–9, https://doi.org/10.1088/1748-9326/aba3d4.
[89] J. Williamson, Low-storage Runge-Kutta schemes, J. Comput. Phys. 35 (1980) 48–56, https://doi.org/10.1016/0021-9991(80)90033-9.
[90] F. Wilmers, Effects of vegetation on urban climate and buildings, Energy Build. (1990) 507–514.
[91] Y. Zhiyin, Large-eddy simulation: past, present and the future, Chin. J. Aeronaut. 28 (2015) 11–24, https://doi.org/10.1016/j.cja.2014.12.007.
[92] F.W. Zwiers, H.v. Storch, Taking serial correlation into account in tests of the mean, J. Climate 8 (1995) 336–351, https://doi.org/10.1175/1520-0442(1995)008<0336:TSCIAI>2.0.CO;2.